Energy & Environmental Science

ROYAL SOCIETY OF CHEMISTRY

PERSPECTIVE

View Article Online
View Journal | View Issue

Check for updates

Cite this: *Energy Environ. Sci.*, 2022, **15**, 5039

Essential data for industrially relevant development of bifunctional cathodes and biopolymer electrolytes in solid-state zinc–air secondary batteries

Domenico Frattini,[a] Estíbaliz García Gaitán,[abc] Ainhoa Bustinza Murguialday,[a] Michel Armand *[a] and Nagore Ortiz-Vitoriano *[ad]

Presently, primary zinc–air batteries (ZABs), with a KOH-based liquid electrolyte, represent the first applied metal–air batteries and the most prevalent non-Li technology. The ZABs' barrier to challenge Li–ion batteries is represented by rechargeability (needing a bifunctional cathode) and durability of the liquid electrolyte (due to leakage and/or evaporation). The liquid electrolyte should be replaced by a solid or gelled one but should not involve fossil-derived polymers or critical ceramic materials. Many naturally occurring biopolymers can be considered to prepare gelled electrolytes for ZABs, but focused literature about synthesis, properties, and applications in ZABs is still needed. Moreover, there is extensive literature about bifunctional cathodes for electrically rechargeable ZABs, but their assessment and performance for further industrialization are insufficient. The bottlenecks of sustainable gel electrolytes, extended cyclability, and relevant depth-of-discharge (DoD) per cycle should be met. In fact, industry seeks rechargeable materials, components, and assemblies capable of providing high current densities (*e.g.*, >5–10 mA cm^{-2}) in long cycles (*e.g.*, >6–12 h) for as large as possible DoD (*e.g.*, >5–10% per cycle, >100% total). The integration in the cells of gelled electrolytes and bifunctional cathode materials could overcome these problems if the correct calculations and testing are performed when carrying out experimental research. In this work, the actual state-of-the-art, key information, limitations, and calculations needed to assess a real promising cell integration between a biopolymer gel electrolyte and a cathode material in, at least, lab scale devices for rechargeability are reported. Finally, a wealth of experimental data spanning cyclability performance at low/medium drain rates (*i.e.*, from 1–2 to 5–10 mA cm^{-2}) at very short cycles (*e.g.*, minutes) and long cycles (*e.g.*, hours), enclosing a DoD analysis, are also shown, serving as a template for future studies.

Received 28th July 2022,
Accepted 29th September 2022

DOI: 10.1039/d2ee02421g

rsc.li/ees

Open Access Article. Published on 13 2022. Downloaded on 11.07.2024 19:25:14.
This article is licensed under a Creative Commons Attribution-NonCommercial 3.0 Unported Licence.

Broader context

Electrochemical energy storage technologies can help mitigate the dependency on fossil sources and greenhouse gas emissions, enabling energy storage from renewable sources and their integration into the grid, thus driving energy transition worldwide. Presently, the most commercialized technology is lithium-ion batteries, from small portable devices to electric vehicles, and up to stationary applications at the grid level. Lithium-ion batteries are characterized by high power and energy density, a high voltage range, and very good rechargeability, thus dominating the field of secondary batteries. However, they are plagued by low environmental compatibility and strong dependency on critical raw materials (CRMs) for which supply chain and/or abundancy are not compatible with sustainable development. Therefore, it is strategically not convenient to rely only on this technology to implement electrochemical energy storage, but few valid alternative candidates can be foreseen considering the electrochemical window and energy density. Zinc–air secondary batteries are one of these; however, affordable development based on industrially and quantitatively relevant breakthroughs is required. In this comprehensive perspective, suitable guidelines are proposed to drive future research in this area, and the most important aspects, advantages, techniques, and testing protocols are critically discussed to make these batteries an attractive reality.

[a] *Centre for Cooperative Research on Alternative Energies (CIC energiGUNE), Basque Research and Technology Alliance (BRTA), Alava Technology Park, Albert Einstein 48, Vitoria-Gasteiz 01510, Spain. E-mail: marmand@cicenergigune.com, nortiz@cicenergigune.com*
[b] *CEGASA Energía SLU, Marie Curie, 1, Parque Tecnológico de Álava, 01510 Miñano, Spain*
[c] *University of the Basque Country (UPV/EHU), Barrio Sarriena, s/n, 48940 Leioa, Spain*
[d] *Ikerbasque, Basque Foundation for Science, María Díaz de Haro 3, 48013 Bilbao, Spain*

Open Access Article. Published on 13 2022. Downloaded on 11.07.2024 19:25:14.
This article is licensed under a Creative Commons Attribution-NonCommercial 3.0 Unported Licence.

1. Introduction

The environmental crisis society is facing has driven us to study high-performance energy generation, conversion, and storage systems.[1] Though lithium-ion technologies continue to top the landscape of rechargeable batteries,[2] primary and secondary zinc–air batteries (ZABs) have made considerable progress in the last decade,[3] advancing at all component levels. Zn-based batteries, and ZABs as well, are not new technologies, but they are being revisited nowadays in the energy storage field as an alternative to lithium ion batteries (LIBs) due to a series of advantages like zinc being an abundant non-critical raw material (CRM), cheap (Li, as battery grade $LiCO_3$, is rated at 75 000 \$ ton^{-1} in 2022,[4] whereas Zn, as a commodity metal, is approx. 3500 \$ ton^{-1} in 2022[5]), and easy to recover/recycle; ZABs use a safe, non-toxic, non-flammable aqueous electrolyte and have interesting specific capacity (theoretically, Li metal is 3860 mA h g^{-1}, Zn metal is $\approx$820 mA h g^{-1}, but practical LIBs are limited to 200–250 W h kg^{-1}, while ZABs can approach 400–450 W h kg^{-1}).[2] However, secondary ZABs suffer from limited voltage, lifetime, cyclability, and rate capability, compared to LIBs. Reliable rechargeability, in ZABs, would be ideal and highly profitable for a valid, economic, and sustainable alternative to LIBs, for portable as well as stationary applications. The main chemical reactions involved in ZABs are:[6]

$$\text{Negative: } Zn + 2OH^- \leftrightarrow ZnO + H_2O + 2e^-,\ E = -1.26\ \text{V } \textit{vs.}\ \text{SHE} \quad (1)$$

$$\text{Positive: } O_2 + 2H_2O + 4e^- \leftrightarrow 4OH^-,\ E = +0.40\ \text{V } \textit{vs.}\ \text{SHE} \quad (2)$$

$$\text{Overall: } 2Zn + O_2 \leftrightarrow 2ZnO,\ E = +1.66\ \text{V } \textit{vs.}\ \text{SHE} \quad (3)$$

where the leftward-going reactions refer to the electrochemical recharge phase in ZABs.

In the actual ZABs' state-of-the-art, the negative electrode (anode during discharge) is based on pure Zn (foil or powder) or Zn alloys (corrosion resistant),[7] the liquid electrolyte is a KOH aqueous solution in the 4–8 M range with dissolved Zn-based salts (acetates, chlorides, or oxides) and additives, and the cathode is composed of a hydrophobic gas diffusion layer (GDL) supported on a soft carbon material (paper, cloth, felt, *etc.*) upon which the active catalyst layer is dispersed. The benchmark positive electrode (cathode during discharge) catalysts are based on platinum group metals (PGMs), especially Pt, Ru, Ir, and their oxides, as well as Co and non-precious transition metal (TM) oxides.[8,9] These oxides, or just the metal atoms, are also variously dispersed on nanostructured carbon materials.[10]

The Zn negative electrode has a complex physico-chemical behaviour, with the main issues being corrosion, hydrogen evolution, dendrite growth, and Zn modifications (*i.e.*, passivation and shape change), which will not be covered here. Alleviating strategies and design concepts are discussed in numerous outstanding studies to which the reader is warmly referred to, for example, ref. 11–14. Liquid electrolytes have always played an essential role in electrochemical energy storage, mainly due to their high ionic conductivities and good contact with electrodes; however, the use of liquid electrolytes entails risks such as leakages and even combustion of organic electrolytes which render them risky for this kind of device. There are other drawbacks of liquid electrolytes such as dendrite growth in liquid solution, which is caused by inhomogeneities that produce preferential nucleation and uneven currents when charging, evaporation and handling issues among others.[15] Therefore, the use of gel polymer electrolytes (GPEs) would be more suitable in electrochemical storage devices. A GPE contains a liquid electrolyte entrapped in a polymer matrix, to retain the ionic conductivity. GPEs eliminate the need for a separator between the two electrodes as the polymer matrix adsorbs the liquid while acting as a physical barrier preventing the internal short-circuit. GPEs have several advantages including safety and resistance against corrosion, excellent flexibility, and processability.[16]

The other pivotal component, that determines the difference between primary and secondary ZABs and between ZABs that are mechanically or electrically rechargeable, is the bifunctional cathode.[17,18] The use of such a cathode enables a simple one-cathode electrode battery design, the absence of a switching system (design with two specialized cathodes), and the absence of complex cases to replace exhausted elements (mechanically rechargeable designs) which makes secondary ZABs compact, easy to connect and operate, and potentially require minimum maintenance.[19] The bifunctional cathode is devoted to the oxygen reduction reaction (ORR) during discharge and the oxygen evolution reaction (OER) during charge. One of the bottlenecks limiting the development of secondary ZABs is the overpotential of the bifunctional catalyst, at discharge as well as at charge. This is a critical aspect of aqueous electrolyte-based batteries because when high currents are applied during cycling, failures occur due to hydrogen evolution or carbon oxidation.[20–23] The same applies to solid and semi-solid gelled electrolytes, where high overpotentials may cause severe deterioration of the gel. The most documented techniques to evaluate the catalyst activity are linear sweep voltammetry (LSV) and cyclic voltammetry (CV) with the rotating disk electrode (RDE). The methodologies, procedures, and selection of the activity metrics in fundamental electrochemical characterization are sources of discussion, hence straightforward comparisons in the literature are often not possible. In early studies, different procedures were adopted, hence some metrics were not defined or available. More comparisons can be found in the supplementary information of a recent work,[24] showing that conditions and RDE loadings may vary, but this has improved recently in new studies. Additionally, projecting encouraging fundamental findings to full cells at the lab scale is not straightforward. The operating conditions of a lab-scale cell might be very different from those of an electrochemical three-electrode cell. This is surely the case of catalysts characterized in a liquid electrolyte, *e.g.*, by RDE in KOH 0.1 M, and then tested in a full cell using a solid GPE. There is an unsaid, non-trivial contribution due to the engineering from the catalyst to the cathode. Generally, these aspects are pertinent also to the anode electrode design (beyond the scope of this work).[11–14]

 This journal is © The Royal Society of Chemistry 2022

Open Access Article. Published on 13 2022. Downloaded on 11.07.2024 19:25:14.
This article is licensed under a Creative Commons Attribution-NonCommercial 3.0 Unported Licence.

In this perspective, GPEs derived from synthetic or natural biopolymers are critically analysed, and their limitations are overviewed; bifunctional cathodes, from catalyst formulation and characterization to electrode design, are discussed and evaluated to guide future work directions. A focused part is devoted to demonstrating, quantitatively, how reliable and usable rechargeability should be assessed to fill the gap between fundamental characterization and testing at the device level, for a market breakthrough, and possible application field expansions envisaged.

2. Biopolymers for gel electrolytes in primary/secondary ZABs

2.1 Naturally occurring *vs.* synthetic biopolymers

In the past decade, research has focused on the design of GPEs for battery applications to replace commonly used liquid electrolytes. The term biopolymers refers to polymers, natural or synthetic, that are naturally degraded and decomposed within a reasonable period of time under environmental conditions by the effect of atmospheric agents, like solar radiation and oxygen, or living agents, like bacteria and enzymes.[25]

Synthetic polymers can be biodegradable, but derive from non-renewable sources totally or partially, depending on the production process. Synthetic polymer gels have found more flexible and diverse biomedical applications[26,27] as well as in several fields[28–30] due to their versatility.[31]

Natural polymers are those derived from natural biomass, animals, or plants and are mainly composed of a few types of repeating carbon-containing chemical building blocks, originating from the cells of living organisms. Naturally occurring biopolymers (*e.g.*, polysaccharides and proteins) have attracted the interest of the scientific community to integrate as GPEs, due to their good biocompatibility, biodegradability, flexibility, mechanical properties, natural abundance, and sustainability. Moreover, they present several reactive sites that can be chemically modified or crosslinked.[32–34]

If the solvent used is aqueous based, the term hydrogel is used to refer to the GPE. Hydrogels are composed of three-dimensional networks that absorb and retain large amounts of water within their solid polymeric matrices.[35] Among GPEs, hydrogels from cellulose, starch, chitosan, and agars are being extensively studied for electrochemical devices.

Naturally derived polymers, however, have a complex structural composition and are therefore difficult to handle and control.[36] As a result, research has mainly focused on developing synthetic biodegradable polymers due to their lower cost and affordability[37] for electrochemical energy storage devices.[38] For example, alkaline GPEs such as polyvinyl alcohol (PVA),[39] polyacrylic acid (PAA),[40] polyacrylamide (PAM), and polyethylene oxide (PEO)[15,41] can be listed.[15]

Much of the early, but also recent, work in metal air batteries (especially in Zn and Na air batteries) has been devoted to the study of synthetic biopolymer-based membranes that act as separators and electrolytes to substitute liquid electrolytes. Recent studies have demonstrated that many biopolymers could be used to obtain semi-solid electrolytes, having a significant impact on the performance of ZABs. The challenge is to develop a gel electrolyte for aqueous systems with stability, conductivity, and physical properties similar to those of organic electrolytes. In the following subsections, synthesis methods, physicochemical properties, and electrochemical performance are summarized to provide at the end a critical outlook of the possible developments.

2.2 Gel biopolymer electrolytes: syntheses and characteristics

GPEs can be synthesized from monomers where the network structure is formed simultaneously during the synthesis and from polymers where the network is obtained by crosslinking the already existing polymer chains.[42]

In this section, current gelation methods and resulting properties are briefly discussed.

2.2.1 Gelation methods: physical and chemical. GPEs can be fabricated by a gelation method followed by immersion in an alkaline liquid electrolyte, or directly formed from an aqueous alkaline solution. There are several methods to obtain hydrogels, but the most used is the solution casting method[39,40,43] which is based on the principle of Stokes' law. Other common methods include electrostatic association, air-drying casting, dipping, extrusion, doping, chemical functionalization,[44] layer-by-layer filtration, phase inversion, and electrospinning.[34,45] In addition, solid particles and/or other additives can be dispersed in the same solution or in a different solution to be mixed later for gelation.[41,46] All these methods can be generally classified based on bonding (physical/chemical crosslinking), or the parameter used to "trigger" gelation (stimuli response). Within the gelation known triggers, a relevant category is that of pH-responsive hydrogels (based on ionic charges).[45]

Selecting the adequate gelation method, to prepare a GPE, is a matter of the specific biopolymer to be used and the degree of bonding to be obtained. It is important to understand these methods to tailor the GPE formulation, fabrication, and properties, but also to exploit diverse and alternative sources of biopolymers.

Bonding nature. In physical gels, the nature of the bonding is due to physical interaction which is normally achieved *via* phenomena such as hydrophobic association, chain aggregation, crystallization, polymer chain complexation, and above all, hydrogen bonding. Physical hydrogels are easy to produce, do not need crosslinking agents during their synthesis and could be reversible due to conformational changes.[34] The methods for producing physically crosslinked hydrogels are ionic interactions, freeze-thawing, stereocomplex formation, non-covalent interaction, and thermoreversible gels.[34] On the other hand, simultaneous gelation/polymerization or post-polymerization gelation is utilized to prepare a chemical hydrogel. In chemical hydrogels, phenomena like covalent crosslinking are utilized for preparation; they are permanent and irreversible because conformational changes are inhibited. They are basically constructed by crosslinking networks; hence, covalent bonds between polymer chains can be established by

Open Access Article. Published on 13 2022. Downloaded on 11.07.2024 19:25:14.
This article is licensed under a Creative Commons Attribution-NonCommercial 3.0 Unported Licence.

the reaction of functional groups. Typical crosslinking agents are glutaraldehyde,[43,47] epichlorohydrin, adipic acid, dihydrazides, *etc.* To chemically crosslink a polymer, grafting, radical polymerization, and condensation reactions can be used.[34,45,48]

Response triggered. Polymers can have a physical (*e.g.*, temperature, pressure, and light), chemical (*e.g.*, pH and chemical initiators), or biochemical response to a trigger. The type of response determines the strength, structure, and properties of the gel. For temperature response, gelation of a polymer by freeze-drying and freeze-thawing techniques is very well known[45] and used for example in PVA hydrogels, providing more porous, spongier, and highly elastic structures.[34,49] Some polymers can be responsive to light, leading to photopolymerization.[50,51] Photopolymerization is an effective method to obtain *in situ* crosslinked (chemical) hydrogels with various architectures in a fairly short time, under solvent-free conditions, at room temperature, or below. The process is typically done in the presence of a photo-initiator upon exposure to a light source (UV or visible), where UV light is the most common one, widely used in industrial processes. There are several photopolymerizable biopolymers that can give hydrogels, such as gelatine, alginate, PEG derivatives, PVA, hyaluronic acid (HA), dextran, cellulose, and chitosan.[50]

pH responsive (ionic charges). Hydrogels with ionic pendant groups can accept or donate protons due to a pH change according to their own degree of ionization (pK_a or pK_b), giving anionic or cationic hydrogels.[45,52] Cationic hydrogels contain pendant groups, such as amine groups, where ionization takes place below the pK_b, which increases swelling due to the increased electrostatic repulsions. These are also known as cation exchange membranes (CEMs), and Nafion and poly(styrene sulfonic acid) are the most common ones which are chemically stable at high acidities; however, the membranes afford low voltage efficiency, even at low working current densities[30] which makes their use in batteries using alkaline electrolytes not suitable. Anionic hydrogels consist of polymer chains functionalized with several groups such as polysulfonium,[53] where deprotonation occurs when the environmental pH is above the pK_a, leading to the ionization of the pendant groups similarly to CEMs, but triggered by a different pH. These are known as anion exchange membranes (AEMs) and most are made from hydrocarbon polymer backbones with covalently attached quaternary ammonium (QA) groups.[44,47,52]

2.2.2 Gel strength, conductivity, and water content. Ionic conductivity, water content, and gel strength are the most important properties when developing a GPE because they determine the fundamental behaviour of the gel. Ionic conductivity is defined as the ion transport capacity in a medium, and it is a key parameter in ZABs[54] because a low resistive OH^- ion transport allows a high conversion rate for the electrochemical reactions.[55] The water content, or water uptake, is defined as the maximum amount of water or alkaline solution that can be retained by the GPE, and hence the number and concentration of charge carriers. Gel strength is important, among other mechanical properties, because it determines the formation of a semi solid electrolyte and governs the mechanical integrity of the finished cell, if there are no other rigid supports (other than the external case). These three properties are somehow interconnected as discussed below.

The ionic conductivity of a solid electrolyte can be enhanced by dissolving *in situ* an alkaline salt into the polymer formulation. Adding *ex situ* KOH solutions (by soaking) will also increase the conductivity, depending on water uptake: GPEs with higher water uptake could benefit from adsorbing lower KOH concentration solutions, while GPEs with limited water uptake would need concentrated KOH solutions to achieve the highest possible ionic conductivity. However, it is reported that at KOH concentrations higher than 6 M, ionic conductivity decreases.[35] The transport easiness of OH^- is associated with its size and its transport *via* the Grotthuss mechanism from one water molecule to the next *via* hydrogen bonding. An increase in temperature causes a faster movement of the anions due to thermal agitation and expansion of ion transport channels, *i.e.*, pores. Plasticizers (*e.g.*, PEG, glycerol, *etc.*[56,57]) can penetrate and alter the cohesive forces between the biopolymer chains, increasing segmental movement, and creating more free volume for ion transport. For liquid electrolytes, ionic conductivity is generally higher compared to that of GPEs.[55] Solid electrolytes lack good ionic conductivity but are easier to manage and reduce leakage and evaporation. The ionic conductivity of some reported GPEs from synthetic and natural biopolymers is shown in Fig. 1.

Water uptake/content is connected to ionic conductivity also due to swelling. The formation of swelling nanochannels in the polymer matrix is significant; the higher the number of pores in the GPE, the easier the transport of OH^-.[54] GPEs with high electrolyte absorption/retention capability act as electrolyte reservoirs also. Low anisotropic swelling boosted the specific capacity and improved the cycling stability of the battery.[54] Good water retention capacity can greatly extend the service life of ZABs that are semi-open systems in which evaporation has a high influence.[58] Thanks to a crosslinked network, hydrogels can absorb and retain a large amount of water.

On the other hand, the higher the crosslinking degree is, the lower the water absorption is.[58] A limited water absorption deteriorates the ionic conductivity, thus leading to early cell failure.[72]

Gel strength has been usually related to the ability of the polymer to form sufficient helical structures for network formation and mechanical stability. Indeed, a linear correlation has been reported between the gel strength and the number of triple helices present in gel-based materials.[73] The gel strength of GPEs from natural biopolymers strongly depends on the specific animal/plant source, the amino acid composition if present, and molecular weight distribution, which differ according to species and the processing conditions, respectively.[74,75] The gel strength also depends on the isoelectric point and can be controlled by adjusting the pH.[55] From pH 4 to pH 9, the strength is not affected to a significant extent. Gels obtained at high alkaline pH (in ZABs the pH is 13–14) generally show

 This journal is © The Royal Society of Chemistry 2022

Open Access Article. Published on 13 2022. Downloaded on 11.07.2024 19:25:14.
This article is licensed under a Creative Commons Attribution-NonCommercial 3.0 Unported Licence.

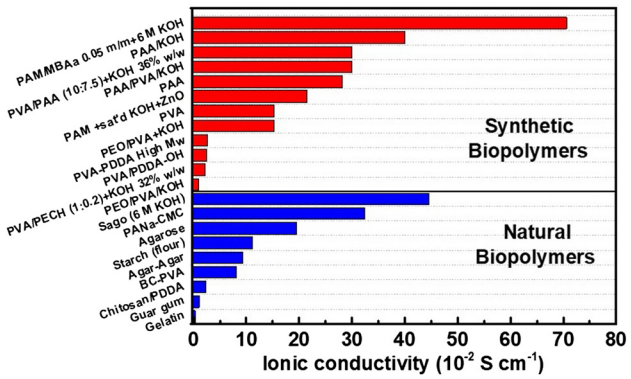

Fig. 1 Bar chart of ionic conductivity for GPEs used in ZABs. Synthetic biopolymers: PAM/MBAa + 6 M KOH;[59] PAA/KOH;[60] PVA/PAA + KOH 36% w/w;[46] PAA/PVA/KOH;[60] PAA;[61] PAM + sat'd KOH + ZnO;[62] PVA;[61] PEO/PVA + KOH;[41] PVA-PDDA High Mw;[63] PVA/PDDA-OH;[64] PVA/PECH + KOH 32% w/w;[65] and PEO/PVA/KOH.[60] Natural biopolymers: sago (6 M KOH);[66] PANa-CMC;[67] agarose;[68] starch (flour);[62] agar–Agar;[69] BC-PVA;[49] chitosan/PDDA;[43] guar gum;[70] and gelatin.[71] PAM: poly(acryl amide); MBAa: *N,N′*-methylenebis-(acryl amide); PVA: poly(vinyl alcohol); PAA: poly(acrylic acid); PEO: poly(ethylene oxide); PDDA: poly(diallyl dimethyl ammonium chloride); PECH: poly(epichlorohydrin); PANa: sodium poly-(acrylate); CMC: carboxymethyl cellulose; and BC: bacterial cellulose.

higher strengths. The gel strength can be enhanced by increasing the density of the internal and surface-crosslinking. The aim of surface-crosslinking technology is to enhance the strength of a gel when it absorbs large amounts of liquid, and various parameters can be adjusted to improve its performance.[73]

Therefore, when designing a GPE, these three properties should be tuned carefully to obtain a good compromise between conductivity, electrolyte retention, and mechanical resistance. The concurrent optimization of these properties is very challenging and is a bottleneck for GPE industrialization because industries and end-users look for ready-to-use performing solutions.

2.3 Current performance of gel electrolytes in ZaBs

GPEs have been earlier tested in primary ZABs and recently they have been proposed also for secondary ZABs, showing interesting performance, in terms of specific capacity, Zn utilization (referred to primary ZABs, and intended as the percentage of zinc utilized and converted to ZnO), and current density. Cyclability needs further effort to be confidently demonstrated (see subsection 3.4 and Section 4), and is more focused on flexible, small devices, showing encouraging performance as power sources for wearable electronics. Although the overall performance strongly depends on anode/cathode materials, cell design, and assembly, GPEs lead to different performances when integrated with ZABs. In primary ZABs:

• Synthetic biopolymer gels obtained from PAA, PVA, and their crosslinked blends give high specific capacities; Zn extraction (calculated as the specific capacity delivered by a fully discharged cell divided by the theoretical capacity of pure zinc, *i.e.*, 819.73 mA h g^{-1}) within 80–90% at current densities from 1–5 mA cm^{-2} and up to 10–50 mA cm^{-2}, in few cases, has been demonstrated.

• Gels from naturally occurring cellulose, nanocellulose, and derivatives usually give good specific capacities, but lower Zn extraction, approx. 70–80%, hardly approaching 85% in few cases.

This was ascribed to the high ionic conductivity of synthetic biopolymer gels, superior water electrolyte uptake, and mechanical strength with small anisotropic swelling.

An overview of the performance of various GPEs in primary/secondary ZABs is given in Table 1. In secondary ZABs, more examples are available for synthetic GPEs whereas a few natural biopolymers (agar-based, cellulose, starches, and gelatines) have been reported. For example, the use of jellified aqueous-based agar–KOH electrolytes has been reported, preventing the water loss due to overcharging and improving the cycle-life and high-charge acceptance. These gels are stable (at near-neutral and alkaline pH) and mechanically flexible, and their ionic conductivity (see Fig. 1) is high enough. Cellulose derivatives have gained immense popularity as gels due to their versatile pH responsive behaviour. Carboxymethyl cellulose (CMC) is an important ionic ether derivative of cellulose and can improve the mechanical integrity of the final film without affecting the ionic mobility and the electrode/electrolyte interfacial characteristics. Moreover, it shows good solubility in water, low cost, biodegradability, biocompatibility, and lack of toxicity.[76] Another commonly used derivative is bacterial cellulose (BC), whose hydrogels have long chains rich in hydroxyl groups, conferring high hydrophilicity. BC hydrogels contain more than 98% of water and exhibit outstanding liquid retention ability.[77]

Although very cheap, the conductivities of these biopolymers are low, and more cell data, as well as fundamental characterization, are needed to assess their potential.[84] For these reasons, the choice by industry of a specific type of GPE is not fixed yet. Going from liquid electrolytes to gels involves making investments in coating technologies that are capital cost intensive. Resorting to chemical crosslinking can be the production rate determining step, and this may become the bottleneck for industrialisation.

2.4 Cell integration: advantages and current limitations

For ZAB technology, strong alkaline GPEs are necessary to provide high ionic conductivity and fast reaction kinetics, while naturally occurring biopolymers can push sustainability.[85] The use of jellified electrolytes for ZABs can improve the performance of these batteries. However, it is still needed to design electrolytes with higher mechanical strengths, temperature tolerance, and high stability during charging to enhance the lifetime of ZABs.

It is also well-known that adding suitable additives to the electrolytes is a straightforward method to reduce the growth of dendrites during cycling.[86] GPEs usually display a lower conductivity compared to liquid electrolytes, but in zinc–ion based technology they are highly desirable because of the protection they offer against dendrite growth due to the superior regulation of Zn cation transport to minimize gradient, and the better current distribution thanks to the nanochannels in the polymer matrix. These effects are supported also by a planar, flat, and homogeneous contact between the GPE and the electrodes.[52] GPEs have good adhesive properties, which provide well-bonded

Open Access Article. Published on 13 2022. Downloaded on 11.07.2024 19:25:14.
This article is licensed under a Creative Commons Attribution-NonCommercial 3.0 Unported Licence.

Table 1 Performances of ZABs with biodegradable GPEs

GPE	Anode/cathode type	ZAB type (primary/secondary)	Performances Primary: current density, specific capacity, discharge time Secondary: current density, cycle time (areal capacity), *n.* of cycles	Ref.
PAA/6 M KOH gel	Electrodeposited Zn/Pt–Ir/C	Primary	1 mA cm^{-2}, ≈700 mA h g^{-1}, — 5 mA cm^{-2}, ≈684 mA h g^{-1}, —	40
PVA/PAA + 32 wt% KOH	Zn powder, carbopol 940, 32 wt% KOH/$KMnO_4$/PTFE/Vulcan C/Ni foam	Primary	PVA : PAA (10 : 7.5): 150 mA (C/10) 1347 mA h, 8.98 h PVA : PAA (10 : 7.5): 300 mA (C/5), 1077 mA h, 3.59 h (theoretical capacity 1476 mA h)	46
Quaternary ammonium functionalized cellulose film + 1 M KOH	Free-standing Zn film/Co_3O_4/carbon cloth	Primary	25 mA g^{-1}, —, 1100 min	54
Starch gel saturated with KOH + ZnO	Zn foil/Mn–Co–Fe@CNT	Primary	2 mA cm^{-2}, 752 mA h g^{-1}, —	62
Sago + 6 M KOH	Zn powder/—	Primary	100 mA, 505 mA h g^{-1}, —	66
PVA/poly(epichlorohydrin) (PECH) + 32 wt% KOH	Zn powder, carbopol 940, 32 wt% KOH/carbon slurry for gas-diffusion, acetylene black and 30 wt% PTFE as a binder	Primary	PVA 150 mA (C/10), 1338 mA h, 8.92 h PVA : PECH (1 : 0.2) 150 mA (C/10), 1290 mA h, 8.60 h (theoretical capacity is 1476 mA h)	65
Quaternary ammonium functionalized cellulose film gelled with 6 M KOH	Free-standing Zn film/Co_3O_4-NCNT	Primary	5 mA cm^{-2}, 652.6 mA h g^{-1}, — 50 mA cm^{-2}, 632.3 mA h g^{-1}, —	78
PVA + KOH	Zn plate in 6 M KOH/Co_4N/CNW/CC P-Co_4N/CNW/CC	Primary	10 mA cm^{-2}, 774 mA h g^{-1}, ≈15 h 50 mA cm^{-2}, 701 mA h g^{-1}, ≈10 h	79
PAA/6 M KOH gel	Electrodeposited Zn/Pt–Ir/C	Secondary	1 mA cm^{-2}, 40 min per cycle (0.33 mA h cm^{-2}), 100 cycles	40
Chitosan and poly(diallyl dimethyl ammonium chloride) (PDDA) + 2 M KOH	Zn foil/IrO_2/Pt/C/carbon paper	Secondary	3 mA cm^{-2}, 10 min per cycle (0.25 mA h cm^{-2}), 16 cycles	43
PVA/guar hydroxy propyl trimonium chloride in 2 M KOH (PGG-GP membrane)	Zn foil/IrO_2/Pt/C/carbon cloth	Secondary	2 mA cm^{-2}, 10 min per cycle (0.167 mA h cm^{-2}), 57 cycles	47
BC-PVA in 6 M KOH + 0.2 M Zn(Ac)	Zn foil/Co_3O_4@Ni foam	Secondary	0.5 mA cm^{-2}, 40 min per cycle (0.167 mA h cm^{-2}), 650 cycles	49
Quaternary ammonium functionalized cellulose + 1 M KOH	Free-standing Zn film/Co_3O_4/-carbon cloth	Secondary	250 mA g^{-1}, 1 h per cycle (125 mA h g^{-1}), 35 cycles	54
Starch gel saturated with KOH + ZnO	Zn foil/Mn–Co–Fe@CNT	Secondary	2 mA cm^{-2}, 10 min per cycle (0.167 mA h cm^{-2}), 216 cycles	62
PVA-KOH (8.3 wt%) PAA-KOH	Zn foil/Co_3O_4/Ag@N-rGO/carbon cloth	Secondary	2 mA cm^{-2}, 10 min per cycle (0.167 mA h cm^{-2}), 100 cycles	61
PAM crosslinked with MBAa in 6 M KOH	Zn foil/C-CoPAN900/carbon paper	Secondary	2 mA, 1 h per cycle, 55 cycles	59
Crosslinked PVA/PAA in 6 M KOH	Zn powder/PEI/Co_3O_4@MWCNT	Secondary	0.5 mA cm^{-2}, 10 min per cycle (0.042 mA h cm^{-2}), 150 cycles	80
PVA-PEO-KOH	Zn foil/$CaMnO_3$-S/carbon cloth	Secondary	5 mA cm^{-2}, 400 s per cycle (0.278 mA h cm^{-2}), 120 cycles	81
PAA + 6 M KOH	Zn foil/Pt/Ru/C	Secondary	0.5 mA cm^{-2}, 10 min per cycle (0.042 mA h cm^{-2}), 25 cycles	82
Quaternary ammonium functionalized cellulose in 6 M KOH	Zinc plate/S-C_2N aerogel/stainless steel mesh	Secondary	25 mA cm^{-2}, 2 h per cycle (25 mA h cm^{-2}), 230 cycles	83

This journal is © The Royal Society of Chemistry 2022

Open Access Article. Published on 13 2022. Downloaded on 11.07.2024 19:25:14.
This article is licensed under a Creative Commons Attribution-NonCommercial 3.0 Unported Licence.

interfaces for the charge and the mass transfer, limiting the dendrite growth and decreasing the corrosion on Zn foils when used as anodes.[16] On the other hand, the extension of the triple-phase boundary zone is generally reduced because of the semi-solid nature of the GPEs.

By cross-linking, it is possible to almost eliminate leakage, retain larger amounts of liquid electrolyte, and increase mechanical resistance, hence the thicknesses of GPEs can be reduced to compensate for the lower ionic conductivity. Comparing the values in Fig. 1, the ionic conductivity of GPEs from synthetic/naturally occurring biopolymers varies within 2 orders of magnitude, depending on the KOH concentration and retention, with higher average values for synthetic GPEs. Mechanical properties, water uptake, biopolymer content, and synthesis determine the ionic conductivity, as explained previously. Oscillations in ionic conductivity are due also to the measurement methodology used to estimate values, because this is not always reported and detailed.

However, reducing the thickness too much, *i.e.*, the distance between the anode and the cathode, without proper physical protection, inherently increases the risk of short circuit and oxygen crossover. For stable and durable ZABs, a uniform and minimized GPE thickness is necessary, considering all the issues mentioned above (*i.e.*, balancing ionic conductivity, internal resistance, mechanical integrity, ion/gas crossover, and dendrite growth). Practicable thicknesses are also dependent on the coating technology available, representing a major investment for companies. Typical thicknesses for advanced fabrication of polymeric membranes and GPEs are in the range of 25–200 μm[52] whereas, by using inexpensive and simple processes, gels with >0.5 mm thickness are prepared. Another drawback in GPEs is the possible dissolution of some metals, *e.g.*, Ni or Mn, from the cathode into the GPEs, or the oxidation of the organic carbon of the biopolymers during the charge phase. For this, less positive voltages at moderate currents for limited charging times should be applied, *i.e.*, lower OER overpotentials. Therefore, the development and modification of hydrogel electrolytes for ZABs, in the aspects of ion conductivity, mechanical properties, environmental adaptability and interfacial compatibility of electrolytes and cathodes still need to be further studied.[87] Several other critical issues await impending solutions, *e.g.*, the CO_2 neutralization toward alkaline electrolytes and temperature adaptability. Blocking CO_2 from the outside environment is challenging, and a possible mitigation strategy is the functionalization of the polymer matrix with specific $-OCO_2^-$ groups.[88] Temperature tolerant ZABs are even more challenging because many polymers give hydrogels non-adaptable to temperature due to the poor interaction between the GPE and the air cathode.[89] The major limit is the aqueous nature of the electrolyte entrapped in the GPE due to freezing below 0 °C and evaporation at high temperature. This can be tackled, for example, by grafting or crosslinking highly polarized functional groups to the polymer matrix thus decreasing the activity of free water molecules in the GPE,[90] or by blending with ionic liquids (ILs).[91]

Positive factors to be considered are the simple preparation process of the electrolytes and their cost. Despite great progress in developing alkaline GPEs, the raw material prices of PVA, PAA, and PAM, for example, are higher compared to those of some biopolymers obtained from natural resources that can be used, like starch-based or agar–agar. Therefore, future directions in this field should make more effort in developing low-cost, affordable, and reliable GPEs[62] by optimizing the conductivity-water uptake-gel strength triad, avoiding carbonate formation by either changing KOH to another salt or implementing selective sieves to reject CO_2 or using non-alkaline pH.

3. Bifunctional cathode materials and extended cyclability

3.1 Trends and development in cathode materials for secondary ZABs

From a rational point of view, it is possible to contemplate as bifunctional catalysts the following options:

- A single compound (multi metallic) capable of catalysing both reactions;
- A mix of two or more compounds/phases, each capable of catalysing the ORR or OER;
- A single support with specific active sites, each capable of catalysing the ORR or OER.

The first option is the straightforward meaning of ''bifunctional'', but it is slightly tricky because the double activity is often more pronounced for one reaction than the other (see subsection 3.3). It can be obtained *via* compositional engineering of materials, such as alloys or ceramic oxides. The second option represents a simple approach based on several combined steps like physical mixing, sonication, mechanochemistry, hydrothermal treatments, *in situ* growth, *etc.*, to prepare composites, from the macro to the nano level, seeking synergies between compounds/phases. The third option is more complex and specifically regards carbon-based catalysts,[92,93] doped with metal atoms and/or non-metal elements like boron, nitrogen, sulphur, and phosphorus. These catalysts can be obtained *via* defect/doping engineering, even from waste biomass as raw carbonaceous materials,[94] showing variety in feedstock, syntheses, and procedures. Active sites can be carbon defects, dispersed single atoms, or small clusters of nanoparticles. An overview of the catalysts recently proposed in the literature for ZABs is shown in Table 2.

The table reports examples of the three options discussed above, and a rough classification by the type of material employed, *i.e.*, metal-free carbon-based,[95] ceramic perovskites,[96] metal/metal oxides over carbons, doped carbons, and nanostructured carbons.[97,98] These catalysts are based on a recurrent group of ''traditional'' elements for this purpose, like Ni, Co, Mn, Ag, Fe, Cu, and rare earths.[9,99] Carbon-based catalysts, doped with N, S, P, or B, and metal atoms (mainly Fe or Co), derived from metal–organic frameworks (MOFs), like zeolitic imidazolate frameworks (ZIFs), are also very popular. Another ''evergreen'' class of

Open Access Article. Published on 13 2022. Downloaded on 11.07.2024 19:25:14.
This article is licensed under a Creative Commons Attribution-NonCommercial 3.0 Unported Licence.

Table 2 Examples of catalysts developed for ZABs in the last decade by the type of material and related syntheses

Type	Cathode materials	Synthesis procedure[a]	Year	Ref.
Composites, nanocomposites	MnO_2/N-CNT	Hydrothermal + CVD + physical mixing	2012	100
	CoO/N-CNT NiFe LDH/CNT	Various steps (Hummer's, precipitation, freeze-drying, and annealing)	2013	101
	Co_3O_4/MnO_2NT	Two-step hydrothermal + calcination	2013	102
	$MnCo_2O_4$/CNT	Various steps (precipitation, hydrothermal, freeze-drying, calcination, physical mixture, and annealing)	2014	103
	$CoMn_2O_4$/N-rGO	Hummer's + two-step hydrothermal	2014	104
	NCNT/CoO–NiO–NiCo	Various steps (coprecipitation, hydrothermal, freeze-drying, and multiple annealing)	2015	105
	Co_3O_4/NPGC	Multistep hydrothermal + annealing	2016	106
	Co-doped TiO_2	Sol–gel	2016	107
	α-MnO_2@XC-72 + $Fe_{0.1}Ni_{0.9}Co_2O_4$/Ti	Coprecipitation	2016	108
	Co_4N/CNW/CC	Various steps (electrodeposition, impregnation, and pyrolysis)	2016	79
	$NiCo_2S_4$/N-CNT	Various steps (Hummer's, precipitation, solvothermal, and freeze-drying)	2017	109
	NiFe-LDH/Co,N-CNF	Various steps (from ZIFs, sol–gel, pyrolysis, etching, and coprecipitation)	2017	110
	Fe@C–NG/NCNTs	Various steps (Hummer's, freeze drying, and pyrolysis)	2018	111
	Mn/Fe–HIBMOFs	Various steps (amination, protonation, oxidation, hydrothermal, and annealing)	2019	112
	FeP–Fe_2O_3/N, P-doped carbon	Coprecipitation, freeze drying, and annealing	2020	113
	FeCo–N–C hollow nanospheres	Pyrolysis + acid leaching of ZIF derived complexes	2021	114
Heterodoped carbons	Fe–N–graphene	Various steps (pseudo-Hummer's, freeze-drying, annealing, physical mixing, and pyrolysis)	2013	115
	N-doped carbon from phenylenediamine	Hard template polymerization + pyrolysis/etching + activation	2014	116
	N-P-C from PANi pyrolysis	Polymerization + freeze drying + pyrolysis	2015	117
	Defective graphene	Multistep pyrolysis	2016	118
	N-doped graphene	Polymerization + pyrolysis	2016	119
	Co-N_x-C/graphene	Various steps (gelification, pyrolysis, leaching, and freeze-drying)	2017	120
	S, N-Fe/N/C-CNT	Precipitation + pyrolysis/leaching	2017	121
	FeCo–N–C	Direct pyrolysis	2017	122
	P, S-CNS	Various steps (precipitation, freeze drying, pyrolysis, *etc.*)	2017	123
	S-doped C_2N aerogels	Various steps (sol–gel, freeze drying, and annealing)	2018	83
	N-doped HPC from raw wood	Enzymatic hydrolysis + pyrolysis	2019	124
	N, S, F-doped carbon	Triazine polymer self-templated carbonization	2020	125
	N, S, P-doped graphene	Ball milling + freeze drying + pyrolysis	2021	126
Perovskite based	$La_{0.6}Ca_{0.4}CoO_3$	Sol–gel	2011	127
	$LaNiO_3$/N-CNT	Hydrothermal + CVD	2012	128
	$La_{1.7}Sr_{0.3}NiO_4$	Sol–gel	2013	129
	$LaNiO_3$/N-CNT	Hydrothermal + CVD	2015	130
	$LaCoO_3$	Sol–gel	2015	131
	$LaTi_{0.65}Fe_{0.35}O_{3-\delta}$/N-doped carbon nanorods	Electrospinning	2015	132
	$La(Co_{0.71}Ni_{0.25})_{0.96}O_{3-\delta}$	Electrospinning	2016	133
	$PrBa_{0.5}Sr_{0.5}Co_{1.5}Fe_{0.5}O_{5+\delta}$ nanofiber	Electrospinning	2017	134
	$La_{0.9}Y_{0.1}MnO$	Sol–gel	2018	135
	$PrBa_{0.5}Sr_{0.5}Co_{1.9}Ni_{0.1}O_{5+\delta}$	Sol–gel	2019	136
	$SrMnO_3$	Sol–gel	2020	137
	$CoS_x/Pr_{0.5}Ba_{0.5}Mn_{0.25}Fe_{0.75}O_{3-\delta}$	Sol–gel + photochemical deposition	2021	138

[a] Common operations like mixing, washing, filtering, centrifugation, *etc.* are not mentioned, for details please refer to the cited references.

catalysts, recently revisited for secondary ZABs, is that of the long-known perovskites and/or ceramic oxides.[100]

In perovskites, recurrent elements are Ni, Co, Mn, Fe, and Cu, with an important use of rare earth elements, especially La, and minor use of alkaline earths like Ca and Sr.

Despite the promising performance and progress in this field, some crucial challenges, at the material and device level, must be undertaken. These can be summarised as follows:

- Cathodes enabling extended cyclability and stability.
- Catalysts with low ORR/OER overpotentials.
- Electrocatalysts based on no/less critical raw materials (CRMs).

Extended cyclability means reliable operations for long cycles (>6 h, up to 24 h per cycle) at 2–5 mA cm^{-2} that can compete with Li-ion technology (see subsection 3.4). Cobalt-containing catalysts have very high and reliable performance, especially for the OER, but Co is listed by the European Union as a CRM, so its availability, supply, and abundance are not compatible with sustainable development.[139] Unfortunately, the same applies to the PGM elements, other elements like Ti, P, and W (relatively abundant but considered CRMs), and

 This journal is © The Royal Society of Chemistry 2022

Open Access Article. Published on 13 2022. Downloaded on 11.07.2024 19:25:14.
This article is licensed under a Creative Commons Attribution-NonCommercial 3.0 Unported Licence.

light rare earth elements (LREE), hence including La, Ce, and Sm. Catalysts based on these elements provide the lowest known overpotentials at the fundamental characterization level, but non-CRM based catalysts could be competitive in real devices. Reducing/eliminating the use of CRMs in cathodes for ZABs will be a major obstacle soon for the development of the technology. In view of the shortage/supply of these raw materials, it is necessary to improve the formulation, atomic structure, and intrinsic/practical activity of catalysts based on no/less CRMs. The future development of cathode materials for secondary ZABs should be focused more to overcome these aspects.

3.2 Essential electrochemical characterization of ORR/OER catalysts

When investigating a new catalyst, it is of primary importance to correctly characterize its activity. This means basically observing the electrochemical behaviour in the form of a current *vs.* potential plot, then correcting potentials and normalizing currents to extract specific curves/values related to independent parameters that characterize the system. Raw data must be always corrected for the deviation of capacitive current effects (a sort of ''background'') and ohmic drops (the so called ''iR'' correction) due to the resistance of aqueous solution, and then potentials referred to the reversible hydrogen electrode (*vs.* RHE) to consider the effect of the pH (and temperature) in alkaline media. The CV and/or LSV techniques, the type of working electrode, RDE and/or the rotating ring disk electrode (RRDE), to perform the basic characterization are consolidated tools.[140]

Considering some of the entries in Table 2, the most popular metrics, together with the RDE mass loading, the electrolyte, and normalization parameters used, are reported in Table 3. The most diffused normalization is based on the geometric area of the RDE working electrode used, and overpotential metrics are the ORR half-wave potential ($E_{1/2}$), the OER potential at a current density j = 10 mA cm^{-2} (E_{10}), both reported *versus* RHE, and the voltage gap between these two points ($\Delta E = E_{10} - E_{1/2}$).

Geometric current density, although very useful at the practical cathode level, is challenging for defining intrinsic activity because bulk and porous catalysts would be normalized to the same value leading to overestimations.[141] An excessive RDE mass loading would lead to a thick layer over the RDE, and electrolyte or oxygen could be accumulated, trapped, and not readily consumed, so an effect of the thickness is observed instead of surface activity.[140,141] $E_{1/2}$ and E_{10} are strongly dependent on a correct RHE conversion, so pH, temperature, and experimental calibration are very important because they determine the exact offset on the potential axis; E_{10} is quite arbitrary, based on geometric current density, and strongly dependent upon RDE mass loading, because of the catalyst's thickness effect due to porosity; ΔE is the difference, so virtually independent of the RHE offset, but it is dependent on the iR correction, and cross comparison between different catalysts is biased by the different surface areas. Therefore, if these popular metrics are being used, all suitable corrections must be done, and the observed currents normalized by the specific surface area obtained, *e.g.*, from BET analysis.[141]

These and further procedural details about RDE experiments, just summarised here, together with benchmarking examples on how to process and report intrinsic activity data, have been excellently discussed in a series of studies[141–144] to which readers are warmly referred to. In general, a golden rule is to seek a mass loading capable of covering completely the working electrode and giving a homogeneous thin film. Of extreme interest is to always report in published studies the rotation speeds, volume and concentration of the electrolyte, the RDE mass loading, catalysts' BET surface areas, pH and temperature used for experiments, the evidence of iR correction (EIS or the value of R) or experimental calibration (CV with a Pt working electrode in pure H_2 and the same cell and electrolyte).

For the ORR and the OER, Tafel plots (semi-log plot of j *vs.* E (*vs.* RHE)) of well-corrected-and-normalized CV/LSV data are warmly recommended as the essential, principal, info required to determine Tafel slopes, a valuable metric to compare activity. When reporting Tafel plots based on specific surface area and catalyst mass, overpotential cross comparisons could be done between different material classes. When comparing current densities, whatever is the normalization used, $E_{1/2}$ is acceptable for the ORR, whereas comparing current densities at a fixed (over)potential *vs.* RHE would be more appropriate for the OER. In the ORR it is possible to have insights by a complete Koutecky–Levich analysis, but the description is beyond the scope of this work. This is necessary to seek/validate enhanced catalysts for the ORR/OER by essential electrochemical characterization.

3.3 Specific activity-driven bifunctional catalyst design: the case of spinel and perovskite-type oxides

To demonstrate how a rational approach and precise electrochemical characterization are fundamental to progress in the field and to provide research directions, the case of spinel (*e.g.*, $NiCo_2O_4$, $MnCo_2O_4$, *etc.*) and perovskite oxide activity determination is critically explained. By correctly applying the corrections and normalizations described in Section 3.2, it is possible to obtain, for each oxide, the specific activity (*i.e.*, current density per specific surface area of the catalyst) as a function of voltage *vs.* RHE. This fundamental information, however, is not able alone to describe, explain, and predict the activity of different oxides. Therefore, the activity was linked to a ''descriptor'' factor, related to the catalyst structure. Many descriptors have been proposed, like the B site-OH bond strength, covalency of metals, and the number of d orbital electrons, giving as a result a characteristic volcano-shaped plot. Finally, the electron occupancy in the antibonding orbitals, e_g, was found to be a key descriptor, applicable to spinel as well as perovskite oxides.[145–147] From these exemplary studies, together with others,[148,149] a critical analysis of the fine volcano plots reported leads to fascinating conclusions on the data available so far:

Open Access Article. Published on 13 2022. Downloaded on 11.07.2024 19:25:14.
This article is licensed under a Creative Commons Attribution-NonCommercial 3.0 Unported Licence.

Table 3 Electrochemical activity metrics, mass loading, electrolyte, and normalization parameters from RDE characterization of bifunctional catalysts for ZABs by the type of material

Type	Cathode material	$E_{1/2}$ *vs.* RHE (V)	E_{10} *vs.* RHE (V)	ΔE (V)	RDE mass loading (mg cm^{-2})	Normalizations and electrolytes	Year	Ref.
Composites, nanocomposites	MnO_2/N-CNT	n.r.[a]	n.r.	n.r.	n.r.	Geometric area, 0.1 M KOH	2012	100
	Co_3O_4/MnO_2NT	n.r.	n.r.	n.r.	0.100	Geometric area, 0.1 M KOH, 2000 rpm	2013	102
	$MnCo_2O_4$/CNT	n.r.	n.r.	n.r.	0.100	Geometric area, 0.1 M KOH	2014	103
	$CoMn_2O_4$/N-rGO	0.80	1.66	0.86	0.900	Geometric area, 0.1 M KOH	2014	104
	NCNT/CoO–NiO–NiCo	0.83	1.5	0.67	0.21	Geometric area, 0.1 M KOH	2015	105
	Co_3O_4/NPGC	0.84	1.68	0.84	0.204	Geometric area, 0.1 M KOH	2016	106
	Co-doped TiO_2	n.r.	n.r.	n.r.	0.108	Geometric area, 0.1 M KOH	2016	107
	α-MnO_2@XC-72 + $Fe_{0.1}Ni_{0.9}Co_2O_4$/Ti	n.r.	n.r.	n.r.	n.r.	Geometric area, 0.1 M KOH	2016	108
	Co_4N/CNW/CC	0.80	1.54	0.74	n.r.	Geometric area, 0.1 M KOH	2016	79
	$NiCo_2S_4$/N-CNT	0.80	1.6	0.80	0.248	Geometric area, 0.1 M KOH	2017	109
	NiFe-LDH/Co,N-CNF	0.79	1.54	0.75	0.120	Geometric area, 0.1 M KOH	2017	110
	Fe@C–NG/NCNTs	0.84	1.68	0.84	0.240	Geometric area, 0.1 M KOH	2018	111
	Mn/Fe–HIBMOFs	0.883	1.51	0.627	0.15	Geometric area, 0.1 M KOH	2019	112
	FeP-Fe_2O_3/N, P-doped carbon	0.838	1.632	0.794	0.255	Geometric area, 0.1 M KOH	2020	113
	FeCo–N–C hollow nanospheres	0.86	1.59	0.73	0.200	Geometric area, 0.1 M KOH	2021	114
Heterodoped carbons	Defective graphene	0.76	1.60	0.84	0.283	Geometric area, 0.1 M KOH	2016	118
	N-doped graphene	0.84	1.66	0.82	0.6 (ORR) 0.3 (OER)	Geometric area, 0.1 M KOH	2016	119
	Co-N_x-C/graphene	0.79	1.74	0.95	0.250	Geometric area, 0.1 M KOH	2017	120
	S, N-Fe/N/C-CNT	0.85	1.60	0.75	0.600	Geometric area, 0.1 M KOH	2017	121
	FeCo–N–C	0.92	1.73	0.81	0.200	Geometric area, 0.1 M KOH	2017	122
	P, S-CNS	0.87	1.56	0.69	0.150	Geometric area, 0.1 M KOH	2017	123
	S-doped C_2N aerogels	0.88	1.53	0.65	0.150	Geometric area, 0.1 M KOH	2018	83
	N-doped HPC from raw wood	0.85	1.68	0.83	0.255	Geometric area, 0.1 M KOH	2019	124
	N, S, F-doped carbon	0.81	1.57	0.76	0.285	Geometric area, 0.1 M KOH	2020	125
	N, S, P-doped graphene	0.82	1.76	0.94	0.200	Geometric area, 0.1 M KOH	2021	126
Perovskite based	$La_{0.6}Ca_{0.4}CoO_3$	n.r.	n.r.	n.r.	0.17–0.24	Geometric area, 1–4–6 M KOH	2011	127
	$LaNiO_3$/N-CNT	n.r.	n.r.	n.r.	1.22	Geometric area, 0.1 M KOH	2012	128
	$La_{1.7}Sr_{0.3}NiO_4$	0.83	n.r.	n.r.	0.141	Absolute current, 0.1 M KOH	2013	129
	$LaNiO_3$/N-CNT	n.r.	n.r.	n.r.	1.22	Geometric area, 0.1 M KOH	2015	130
	$La(Co_{0.71}Ni_{0.25})_{0.96}O_{3-\delta}$	n.r.	1.554	n.r.	0.700	Geometric area, mass, 0.1 M KOH	2016	133
	$PrBa_{0.5}Sr_{0.5}Co_{1.5}Fe_{0.5}O_{5+\delta}$ nanofiber	0.73	1.53	0.80	0.796	Geometric area, 0.1 M KOH	2017	134
	$La_{0.9}Y_{0.1}MnO$	0.75	n.r.	n.r.	0.236	Geometric area, 0.1 M KOH	2018	135
	$PrBa_{0.5}Sr_{0.5}Co_{1.9}Ni_{0.1}O_{5+\delta}$	n.r.	n.r.	n.r.	0.796	Geometric area, 0.1 M KOH	2019	136
	$SrMnO_3$	0.81	n.r.	n.r.	0.25	Geometric area, mass, 0.1 M KOH	2020	137
	$CoS_x/Pr_{0.5}Ba_{0.5}Mn_{0.25}Fe_{0.75}O_{3-\delta}$	0.70	1.56	0.86	0.226	Geometric area, 0.1 M KOH	2021	138

[a] n.r. = not reported; the values are not available *vs.* RHE, not defined, not measured, not explicitly mentioned, or cannot be reliably calculated from the reference. For details, please refer to the cited reference.

• Oxides with the same value of e_g can present small or even relevant different activities. A reason could be due to particle size, morphology, and shape, other than the stoichiometry and chemical formula, hence could be optimized. It is also known that, depending on the overlap degree of the O–2p orbitals with the orbitals of the atom in the active site, the spin state and e_g can change;

• Considering the reported oxides, the same oxide, although presenting a relevant bifunctionality, could show different activities for the ORR and the OER, hence it is not the ''best in class'' for both reactions;

• Doping the basic ABO_3 structure of a specific perovskite by introducing another element in the A and/or B site can alleviate this activity discrepancy between the ORR and the OER, reducing the relative difference between the overpotentials;

• Although doping could balance and leverage the bifunctionality of the oxide, it does not always reduce the absolute overpotentials; hence, there are combinations of elements that work better than others and oxygen-defective oxides seem to display improved activity;

• The theoretical vertexes of the volcano plots for the ORR and the OER seem to fall at different values of e_g (in perovskites, for the ORR, the max activity should be around e_g 0.71,[145] for the OER at around 1.25[146] or 1[150]), depending on current density, hence a single oxide cannot be the best for both

Open Access Article. Published on 13 2022. Downloaded on 11.07.2024 19:25:14.
This article is licensed under a Creative Commons Attribution-NonCommercial 3.0 Unported Licence.

reactions, but just as close as possible to both values (the mathematical averages being 0.98 or 0.86);

• However, the exact position of the top of the volcano could depend on the number of data points, *i.e.*, the number of perovskite oxides, the precision in the measurement of e_g, especially for solid solutions, *i.e.*, doped systems, and the current density at which potentials or overpotentials are taken, *i.e.*, the Tafel slope somehow.

Therefore, although being a powerful descriptor tool, it is not faultless; it is not the only one, and should not be used alone, but for sure can guide and unify future research on specific directions, like the development of new syntheses, active materials with no/less CRMs, and their correct activity classification within the field. By accepting a descriptor as robust and reliable, and considering these observations, future research trends, with a solid basis, can be proposed to achieve fundamental progress in electrocatalysis as well as materials science.

3.4 From catalysts to cathodes: electrode design and performance evaluation for scale-up

Upscaling electrocatalysis findings is not straightforward because a cathode, at the full cell level, may have different properties (thickness, porosity, formulation, *etc.*), far from the catalyst powders used for the RDE. The cathode is a structured full-scale component, of which the bifunctional catalyst is a part, and it is composed of the following elements (with relative functions):

• Conductive support/filler (*e.g.*, carbon paper, metal mesh, and/or carbon powder): serving as the main structural part to convey/distribute charges, in the form of ions and/or electrons, from the electrolyte/external circuit. It is characterized by electrical conductivity, porosity, and wettability (*i.e.*, hydrophobic/hydrophilic behaviour).

• Current collector (*e.g.*, Ni wires): serving as the component to collect electrons from/to the cathode. It can be a physically separated piece, hence just in contact with the cathode, or integrated, welded directly to the supporting metal mesh, if any, thus effectively becoming the collector and support of the cathode.

• Gas diffusion layer (GDL): serving as a hydrophobic barrier, obtained by depositing/painting/mixing, for example, poly(tetrafluoroethylene) (PTFE) with the conductive support. It also has a binder function when used in the form of powder/solution and mixed with the catalyst. It can prevent liquid electrolyte leakage/evaporation and can facilitate oxygen transport from air to the catalyst, and *vice versa*.

• Catalyst layer: serving as the active material where the cathodic discharge/charge half reaction takes place. As in the air electrodes of other technologies (*e.g.*, fuel cells[151]), around the particles of the catalyst, the critical three-phase boundary (TPB) zone is formed.

The formation of an extended and favourable TPB zone is the microscopic result of the electrode design, *i.e.*, the integration of the different parts listed above, because all of them contribute to the contact with the electrolyte. At the engineering design level, some aspects to be carefully considered are:[151]

• Selection of materials (for the conductive support, current collector, GDL, catalysts).

• Formulation (*e.g.*, catalyst loading, binder amount, and other additives).

• Wettability and porosity (*e.g.*, to control the flooding of electrolytes, leakage, evaporation, oxygen crossover, *etc.*).

• Processing (final thickness, surface finishing, geometry, and homogeneity).

In cathode design, selection and formulation are related to the intrinsic electrochemical behaviour, while the other two determine the physical behaviour, especially the balance between the hydrophobicity and hydrophilicity of the surface in contact with the electrolyte, and oxygen diffusion *vs.* oxygen barrier of the surface exposed to air.[152] In alkaline media, it is believed that the hydrophobic portion of the cathode, with catalytic sites exposed, is involved in the ORR, whereas the hydrophilic portion, with relevant catalytic sites, participates in the OER (Fig. 2).

This concept led to the separation (decoupling) of cathode functions, *i.e.*, discharge/charge, together with the formation and control of separated hydrophobic and hydrophilic portions within the same cathode.[152,153] The consequence is an asymmetric design in terms of material composition and wettability[152,154] that is capable of extending the reactive interface from a 2D to a 3D multiphase interface.[154,155] This is further complicated in ZABs with solid or gelled electrolytes because the physical surface in contact with the cathode is smaller, hence the porous structure, channel networks for mass transport and the number of available active sites for the reactions must be strictly controlled, together with flexibility and mechanical strength in the case of flexible ZABs.[156] Another example is the interference of non-catalyst components on the OER during the charging process. It is true that, during the charging process, some current collectors and electrical contacts (*e.g.*, stainless steel, Ni-based, *etc.*) are not inert due to the applied oxidizing potentials, possibly interfering with the OER process.[157] Resistance to the corrosion and oxidation of the electrocatalyst, as well as of the conductive support or current collectors, is critical for stability and rechargeability.

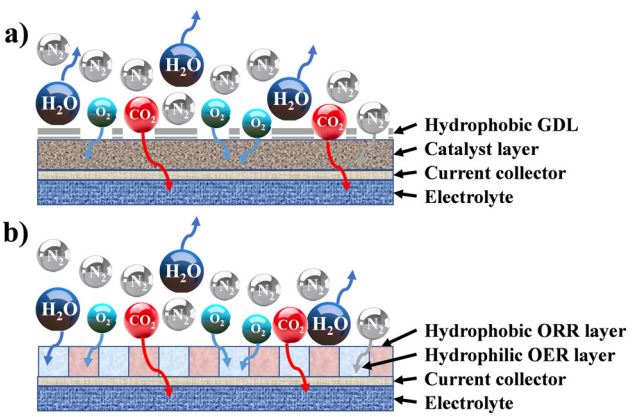

Fig. 2 Architecture of a gas diffusion electrode: (a) standard structure (coupled ORR/OER activity); (b) decoupled ORR/OER hydrophobic/philic structure.

Open Access Article. Published on 13 2022. Downloaded on 11.07.2024 19:25:14.
This article is licensed under a Creative Commons Attribution-NonCommercial 3.0 Unported Licence.

Apart from materials selection, *i.e.*, carbon conductive additives, the addition of a protective layer, corrosion resistant current collectors, *etc.*, the issue is mitigated, and electrocatalysts' stability is improved, if the overpotential at charging is reduced (as measured from LSV by the RDE). Therefore, electrocatalyst stability should be tested alone, without interfering agents, and cathode corrosion resistance, during charging, could be checked considering different designs and formulations of the electrode. This is necessary for the correct estimation of stability in the long term, and to distinguish the intrinsic behaviour of the catalyst from the other components of the electrode. These are some of the challenges when scaling up catalysts to cathodes, creating discrepancies with the results from fundamental electrochemical characterization.

Considering a potentially interesting novel catalyst, with encouraging intrinsic activity determined by suitable descriptors, a poor electrode design, in cathodes bearing the novel catalyst, could invalidate the encouraging fundamental results. On the other hand, a poor performance evaluation of full cells with novel cathodes can lead to hyped claims, not reflecting device-relevant performance for lab-scale cells as well as scaled-up batteries. When considering performance evaluation, cells must be studied as a whole, and any information about their components (dimensions, weights, formulations, *etc.*) should be provided and mentioned to conduct a proper evaluation.[158] All the components contribute to the overall performance of the cells, even if the only component varied in a study is the cathode. Testing relevant cycling conditions is also necessary to validate the real benefits and improvements due to the catalyst as well as the electrode and cell design. In the work of Parker *et al.*,[2] this issue is addressed, and guiding equations are provided to formulate convincing and solid protocols for performance evaluation. Here, the most important equations are analysed, further elaborated, and critically commented. The main descriptor of performance for a ZAB is the depth of discharge (DoD) of zinc, the only active material stored in the battery (O_2 is not stored inside the battery and is virtually "infinite"). The DoD is defined as the ratio between the capacity extracted from the battery and the capacity theoretically available from the active material, and is given by:[2]

$$\mathrm{DoD_{Zn}} = \frac{A_j \times j \times t}{m_{\mathrm{Zn}} \times 819.73} = \frac{A_j \times j \times t}{A_{\mathrm{Zn}} \times h_{\mathrm{Zn}} \times \rho_{\mathrm{Zn}} \times 819.73} \quad (4)$$

where A_j is the geometric area (anode, cathode or else) used to normalize the current density j, t is the total discharge time, m_{Zn} is the total mass of zinc inside the battery, A_{Zn} is the geometric area of the zinc electrode, h_{Zn} is the thickness of the zinc electrode, ρ_{Zn} is 7.13 g cm^{-3} the density of metallic zinc, and 819.73 mA h g^{-1} is the theoretical specific capacity by mass of zinc. It is worth noting that this is a macroscopic equation, based on operating and physical quantities, it does not give/require specific information about catalyst activity, physical properties, *etc*. As soon as the geometry of the anode electrode, the effective zinc mass, and cycling conditions, *i.e.*, current density and time, are known, the $\mathrm{DoD_{Zn}}$ can be easily calculated. By considering a single discharge/charge cycle, with current density j and discharge time per cycle t_{dis}, in a battery assembled with a mass of zinc m_{Zn}, the total DoD, $\mathrm{DoD_{tot}}$, and the DoD per cycle, $\mathrm{DoD_c}$, can be easily defined and calculated as:

$$\mathrm{DoD_c} = \frac{A_j \times j \times t_{\mathrm{dis}}}{m_{\mathrm{Zn}} \times 819.73} \quad (5)$$

$$\mathrm{DoD_{tot}} = n_{\mathrm{c}} \times \frac{A_j \times j \times t_{\mathrm{dis}}}{m_{\mathrm{Zn}} \times 819.73} = n_{\mathrm{c}} \times \mathrm{DoD_c} \quad (6)$$

where n_{c} is the number of cycles performed by the cell. When a cell is assembled, and the cycling conditions are selected, $\mathrm{DoD_c}$ can be calculated *a priori* from eqn (5), n_{c} being the only unknown for $\mathrm{DoD_{tot}}$. Therefore, the number of cycles is important and is frequently used in the literature as an indicator of performance but might not be enough. Usually, it is hard to retrieve information about the exact amount of zinc used or the geometry of the cell, so the DoD cannot be precisely calculated. To avoid misunderstanding, the geometric areas involved must be clearly stated to facilitate DoD calculation. In eqn (4), if A_{Zn} is used to normalize the current density, or if $A_{\mathrm{Zn}} = A_{\mathrm{cathode}}$, the $\mathrm{DoD_c}$ depends only on cycling conditions (j and t_{dis}), and h_{Zn}, hence the $\mathrm{DoD_c}$ can be modulated by changing the cycling or by changing the design, *i.e.*, geometry, of the anode. Similarly, if $A_j = A_{\mathrm{cathode}}$ and $A_{\mathrm{cathode}} > A_{\mathrm{Zn}}$, to a certain extent the $\mathrm{DoD_c}$ could be increased by changing cell design and geometry. However, a limit of this approach is that it is not possible to know at the microscopic scale what will be the effect of different geometries on charge transport due to the area mismatch. Another interesting observation proposed in Parker *et al.*[2] refers to the cycling conditions, namely the product $j \times t_{\mathrm{dis}}$. The authors claim that for a rechargeable ZAB to be competitive with a Li-ion battery, at the cell level, this product should exceed the value of 11.7 mA h cm^{-2}, and the DoD should exceed 20% (when a very thin Zn foil is used as the anode). Hence, the selection of suitable cycling conditions is also critical in performance evaluation for reliable scale-up.

Another notable example of performance is given by the calculation of the total specific energy[2] and specific energy per cycle, both in W h kg^{-1}:

$$\text{Specific energy}_{\mathrm{c}} = 819.73 \times \mathrm{DoD_c} \times f_{\mathrm{Zn}} \times V_{\mathrm{avg}} \quad (7)$$

$$\begin{aligned}\text{Specific energy}_{\mathrm{tot}} &= n_{\mathrm{c}} \times \text{Specific energy}_{\mathrm{c}} \\ &= n_{\mathrm{c}} \times 819.73 \times \mathrm{DoD_c} \times f_{\mathrm{Zn}} \times V_{\mathrm{avg}}\end{aligned} \quad (8)$$

where V_{avg} is the average discharge voltage of the ZAB, and f_{Zn} is the weight fraction of zinc in the assembled cell, calculated as:

$$f_{\mathrm{Zn}} = \frac{m_{\mathrm{Zn}}}{m_{\mathrm{anode}} + m_{\mathrm{cathode}} + m_{\mathrm{electrolyte}}} \quad (9)$$

where m_{cathode} is the total mass of the cathode electrode, $m_{\mathrm{electrolyte}}$ is the total mass of the electrolyte, and m_{anode} is the total mass of the anode (it can be different from m_{Zn} in case pure zinc is not used). Eqn (7)–(9) have been slightly modified from those in Parker *et al.*[2] and adapted to a lab-scale single cell to calculate energy density. Versions for scaled-up battery packs

 This journal is © The Royal Society of Chemistry 2022

Open Access Article. Published on 13 2022. Downloaded on 11.07.2024 19:25:14.
This article is licensed under a Creative Commons Attribution-NonCommercial 3.0 Unported Licence.

can be found in the mentioned work. Also, in this case it is evident that, if not all the masses are reported, it will be not possible to precisely calculate the specific energy/energy density by mass. Moreover, design engineering here is important to optimize the components' weight and maximize f_{Zn}.

Although the equations presented here, and the others in the mentioned work, do not offer a relationship between the macroscopic and microscopic behaviours of each component, they can describe, at least, the effect of improved cell and cathode electrode designs. Viable directions are the mixing of two specialized catalysts, one for the ORR and one for the OER, with the lowest overpotentials, using a corrosion resistant additive and a structured GDL, capable of balancing hydrophobic and hydrophilic zones with the active sites, into a robust thin electrode to optimize weight and thickness for a compact design. This will increase f_{Zn}, V_{avg}, round-trip efficiency, and therefore energy density.

4. Cell integration and perspective performance for extended cyclability

In this section, experimental cyclability data for electrically rechargeable ZABs are shown and briefly discussed. The aim is to compare the behaviour under very short/long cycles (*i.e.*, small/large areal capacity) to understand the current limitations. The anode is obtained by mixing commercial zinc powder (Zn > 99%, Cegasa, Spain) and a 45% w/w KOH solution (KOH pellets, >99%, Scharlab, Spain) to form a paste with 65% w/w of active zinc. The electrolyte is a semi solid GPE patent pending, containing KOH and a naturally occurring biopolymer. The bifunctional cathode is a mixture of a MnO_2/carbon/PTFE primary catalyst (Cegasa, Spain), nickel cobalt oxide (NCO, $NiCo_2O_4$, >99%, Sigma-Aldrich, Germany), and ethanol in a 1 : 1 : 1 mass ratio to obtain a paste that is then pressed on a Ni mesh and dried at 60 °C overnight. A home-made design, consisting of a Teflon case with circular compartments for the components, was used. Anode paste fills a 13 mm in diameter compartment; upon it a GPE disk of 24 mm in diameter is placed, and then a 20 mm diameter MnO_2/NCO on Ni mesh disk cathode (area 3.14 cm^2) completes the stack. Ni-based current collectors/wires are placed as electrical contacts. The cell is closed by a Teflon cap with passing-through aeration holes, held in place by an O-ring and two bolts. The current density is normalized by the anode geometric area (1.33 cm^2) and the specific capacity is normalized by the precise mass of active zinc used. The cells are tested in a constant current mode (CC) in a BCS 815 potentiostat (BioLogic, Seyssinet-Pariset, France), and cycles are defined as symmetric discharge/charge. The cutoffs are set at 0.8 and 2.0 V *vs.* Zn/Zn^{2+}, for discharge and charge, respectively. Once the exact amount of active zinc is known, together with the weights of the electrolyte and the cathode, the information given above is sufficient to apply all the equations reported in subsection 3.4 to perform a consistent evaluation of the results.

4.1 Cyclability analysis and DoD for short cycles

A very commonly used cycling condition, especially for aqueous ZABs, is 10 min per cycle, *i.e.*, 5 min discharge and 5 min charge, at a current density of 5 mA cm^{-2}. This is equal to an areal capacity of 0.416 mA h cm^{-2}. By assembling a cell as described above, and cycling it under these conditions, a voltage profile is shown in Fig. 3.

In Fig. 3, the voltage profile was divided into three regions to consider the change in the discharge voltage, due to a large number of cycles, and almost stable discharge/charge cycles. Between each region, there was a resting time in open circuit voltage mode overnight, and it was possible to relaunch the same cell twice. Under the same conditions (with no resting time), and using the same materials, duplicated cells gave an average number of cycles of 2500–3000 (see Fig. 5 in the next subsection). The cell above is used as an example to explain the cumulative effect of the number of cycles on metrics, the effect of resting time will be studied in future works. According to eqn (4)–(9), using a specific capacity of 819.73 mA h g_{Zn}^{-1}, and the voltage profile in Fig. 3, the following figures can be calculated.

Although there are no formal definitions of short and long cycles, considering a threshold of ≈12 mA h cm^{-2} suggested by Parker *et al.*,[2] and current densities suitable with ZABs, 0.416 mA h cm^{-2} is a very small value due to the small discharge/charge time, hence is referred to as a (very) short cycle. The DoD per cycle is therefore very small, but it depends also on the active zinc mass. With a small areal capacity, high DoD can be achieved by using less zinc, but anyway this discharge time has no practical application at the device level. Both parameters should be taken into consideration when setting cycling conditions. For energy, by using the weights, DoD_c, and n_c in Table 4, the specific capacity (819.73 mA h g_{Zn}^{-1}), and the voltage profiles in Fig. 3, the figures in Table 5 are calculated.

The cumulated figures are really promising, showing interesting values for the total DoD, n_c, and specific $energy_{tot}$.

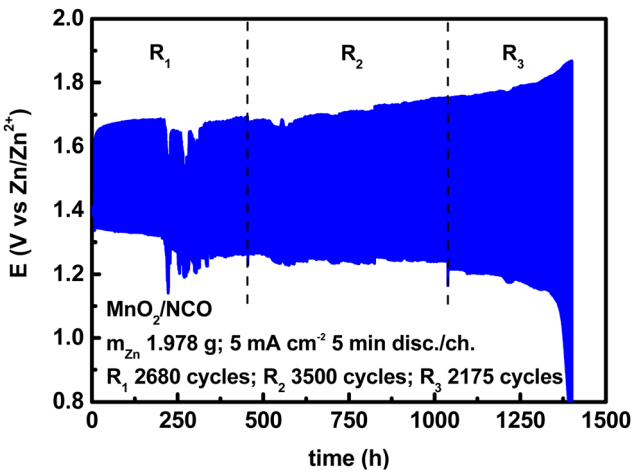

Fig. 3 Electrically rechargeable ZABs (anode paste, GPEs from natural biopolymers, bifunctional cathodes) operated under "short cycles".

Open Access Article. Published on 13 2022. Downloaded on 11.07.2024 19:25:14.
This article is licensed under a Creative Commons Attribution-NonCommercial 3.0 Unported Licence.

Table 4 Cyclability analysis of three regions at 0.416 mA h cm^{-2} (5 mA cm^{-2}, 5 min discharge/charge)

Region	m_{anode} (g)	m_{Zn} (g)	$m_{electrolyte}$ (g)	$m_{cathode}$ (g)	n_c (−)	DoD_c (%)	DoD_{tot} (%)
R_1	2.931	1.978	1.626	0.495	2680	0.034	91.120
R_2	2.931	1.978	1.626	0.495	3500	0.034	119.000
R_3	2.931	1.978	1.626	0.495	2175	0.034	73.950
Overall	2.931	1.978	1.626	0.495	8355	0.034	284.070

However, this is an effect of the number of cycles, because the figures per cycle, DoD_c and specific $energy_c$, are low. The DoD per cycle can be improved by optimizing/minimizing the mass of zinc, but to a limited extent. In Table 4 a large mass of zinc paste is used, whereas thin zinc foils are widely used in the literature. Considering a zinc density of 7.13 g cm^{-3}, $A_{cathode} = A_{anode} = 1$ cm^2, and the same areal capacity of 0.416 mA h cm^{-2}, prospective DoD_c (eqn (5)) by changing foil thickness is given in Table 6.

As expected, by reducing the foil thickness, for constant areal capacity and cycling conditions, zinc mass decreases, the available theoretical capacity decreases, and DoD_c increases. However, for full cells, the real cycling feasibility of very thin zinc foil anodes must be proven. The last example of a 10 μm thick zinc foil, giving 7.25% of DoD each cycle of 5 min discharge per 5 min charge at 5 mA cm^{-2} is just a calculation, showing that even by reducing thickness, an interesting DoD_c is not met anyway. The only other way to increase the DoD_c is to increase the areal capacity or at least to increase the discharging/charging time. Something similar was also claimed by Parker *et al.*,[2] together with the doubt that these ''short cycles'' are more useful as fundamental electrodeposition study rather than device-relevant testing. In this regard it must be also added that in liquid electrolyte secondary ZAB tests in the literature, the KOH-based electrolyte also contains zinc acetate or zinc chloride, very frequently at 0.2 M. This means that, other than zinc foil, Zn is also present as a cation or as $Zn(OH)_4^{2-}$ derived from the action of KOH, at an equivalent zinc concentration of approx. 13 mg mL^{-1} in the liquid, giving an equivalent extra capacity of 10.6 mA h mL^{-1}. In the GPE used in the cell shown in Fig. 3 there is no extra zinc. Depending on the amount of zinc, foil thickness, and the volume of liquid electrolyte, a non-negligible source of extra capacity (approx. 6–18% per mL, with Zn foil of 0.1–0.3 mm thickness and active area of 1 cm^2) coming from the liquid could participate in the Zn deposition during charge, especially if the areal capacity, discharging/charging times, and DoD_c are small (hence, the zinc foil could be under-used or misused). Therefore, it is extremely important to clearly report the geometry/area of electrodes, which one is used to calculate current density, and the total weight of the anode and active zinc, at least.

Table 5 Energy analysis of three regions at 0.416 mA h cm^{-2} (5 mA cm^{-2}, 5 min discharge/charge)

Region	V_{avg} (V)	f_{Zn} (−)	Specific $energy_c$ (W h kg^{-1})	Specific $energy_{tot}$ (W h kg^{-1})
R_1	1.300	0.392	0.142	380.560
R_2	1.250	0.392	0.137	479.500
R_3	1.200	0.392	0.131	284.925
Overall	1.250	0.392	0.137	1144.985

4.2 Long cycles at higher DoD for battery-relevant performance

When the areal capacity is increased at cycling, the performance starts fading, and the figures from cyclability and energy analyses are less encouraging. In this work some larger cycles, at higher areal capacities, have been tested using the same materials and assembly. Voltage profiles for three different areal capacities are given in Fig. 4.

As expected, by increasing the areal capacity, especially discharge/charge time, the number of cycles drastically decreases from thousands to a few cycles. On the other hand, DoD_c and specific $energy_c$ increase, and the discharge times are compatible with portable or stationary applications (*i.e.*, hours). Cyclability and energy calculation for the three examples in Fig. 4 are reported in Table 7.

The cumulated figures in these cases are lower than those in Tables 4 and 5 mainly due to the small number of cycles, while the amount of active zinc is reduced, areal capacity is increased, and hence DoD_c and specific $energy_c$ increased substantially. These conditions are more attractive for practical applications at the device level; the challenge is thus to increase under these cycling conditions the number of cycles, the total DoD, and hence the total specific energy.

Another aspect emerging from these data, to be highly considered, is that the electrical rechargeability of a lab-scale device can be improved by optimizing the cell design. In fact, in all the examples, the materials used are the same but components' weights change (affecting directly f_{Zn}, DoD_c, and indirectly the others), and the electrode area of the home-made cell used are different (anode 1.33 cm^2 *vs.* cathode 3.14 cm^2) not directly affecting any calculation (the area used here for current density is always the anodic one), but operations (*i.e.*, real current density experienced by the anode during discharge and by the cathode during charge may differ). Materials science

Table 6 Prospective DoD_c for common zinc foils and ''short cycles''

Foil thickness (cm)	Area (cm^2)	Volume (cm^3)	Mass (g)	Theoretical capacity (mA h)	Areal capacity (mA h cm^{-2})	DoD_c (%)
0.030 (300 μm)	1	0.030	0.214	175.422	0.416	0.237
0.020 (200 μm)	1	0.020	0.143	117.221	0.416	0.355
0.010 (100 μm)	1	0.010	0.071	58.200	0.416	0.715
0.001 (10 μm)	1	0.001	0.007	5.738	0.416	7.250

 This journal is © The Royal Society of Chemistry 2022

Open Access Article. Published on 13 2022. Downloaded on 11.07.2024 19:25:14.
This article is licensed under a Creative Commons Attribution-NonCommercial 3.0 Unported Licence.

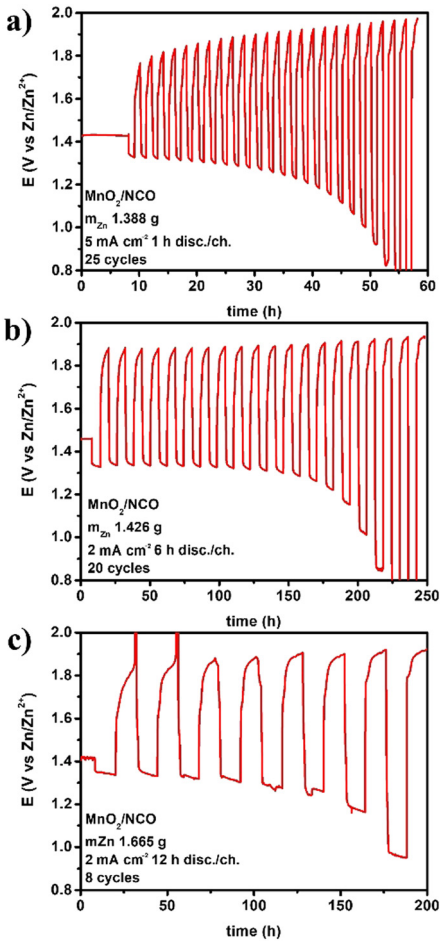

Fig. 4 Electrically rechargeable ZABs (anode paste, GPEs from natural biopolymers, bifunctional cathodes) operated under "long cycles" at (a) 5 mA h cm^{-2}, (b) 12 mA h cm^{-2}, and (c) 24 mA h cm^{-2}.

(for anodes, electrolytes, and bifunctional catalysts), engineering design (for each component, single cell geometry, and assembly), and electrochemistry (for cycling conditions, operating strategy during discharge/charge) are highly connected, all affecting the figures reported. Other areal capacities have been explored in this work, and the trend n_c *vs.* areal capacity is shown in Fig. 5.

Future development of electrically rechargeable ZABs should aim therefore to improve and assess enhancement in materials, design, and testing of devices considering all these parameters to achieve more cycles at higher areal capacities (hence $DoD_{tot} > 100\%$, meaning real recharge).

According to the literature and the threshold recommended,[2] three areal capacity regions are suggested here: very low (from 0 to 2 mA h cm^{-2}), medium (from 2 to 12 mA h cm^{-2}) and very high (>12 mA h cm^{-2}) regions, based on areal capacity, and supposing that current densities are in the range of 1–5 mA cm^{-2} and the discharge/charge time is in the range of a few hours. This is because high current densities, especially at charge, are associated with various failure mechanisms,[1] as well as long cycling time could lead to dendrite formation, if not suppressed.[159] The DoD per cycle is also connected to this map but, apart from areal capacity, it depends on the structure, geometry and active zinc mass in the single cell,[159] shaping the voltage profile when it is the limiting electrode in the device.[107,160]

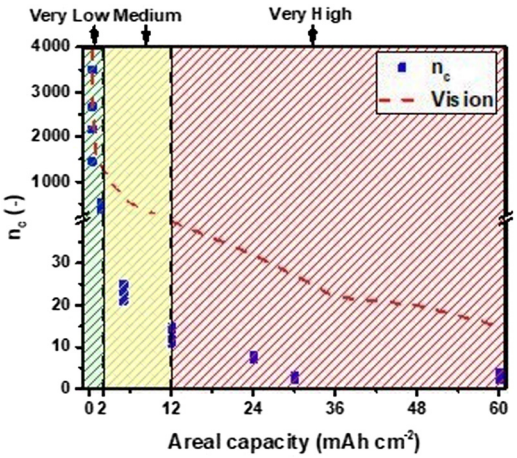

Fig. 5 Number of cycles, n_c, *vs.* areal capacity trend with prospective development for electrically rechargeable ZABs.

5. Current and potential applications for primary/secondary ZABs

Following the discussion in previous sections about the research and development of ZABs, it is critical to reflect on the progress made in fundamental studies into field applications and relevant environments. Considering the technology readiness level (TRL) scale, this means performing the "hard jump" from TRL 1–3 to TRL 4–6 and beyond. For electrically rechargeable ZABs this is actually the most limiting aspect for prospective development toward commercialization, delayed also by the unreconciled validations of integrated cells. The existing applications for primary and secondary ZABs are overviewed below, together with the possible expansion of the field if the challenges discussed for GPEs and bifunctional cathodes are resolved.

Table 7 Cyclability and energy analysis for electrically rechargeable ZABs during "long cycles"

Areal capacity (mA h cm^{-2})	m_{anode} (g)	m_{Zn} (g)	$m_{electrolyte}$ (g)	$m_{cathode}$ (g)	n_c (–)	DoD_c (%)	DoD_{tot} (%)	V_{avg} (V)	f_{Zn} (–)	Specific $energy_c$ (W h kg^{-1})	Specific $energy_{tot}$ (W h kg^{-1})
5	2.056	1.388	1.889	0.457	25	0.585	14.625	1.200	0.315	1.813	45.325
12	2.112	1.426	1.507	0.487	20	1.366	27.320	1.250	0.347	4.857	97.140
24	2.467	1.665	1.646	0.563	8	2.338	18.704	1.260	0.356	8.597	68.776

Open Access Article. Published on 13 2022. Downloaded on 11.07.2024 19:25:14.
This article is licensed under a Creative Commons Attribution-NonCommercial 3.0 Unported Licence.

5.1 Primary ZABs in portable applications

Today, primary ZABs are a commercial reality, with a TRL 9, but are limited to their initial market niche of power sources for hearing aid devices. The field of portable applications, including secondary cells, is today an unconquerable domain of LIBs and other intercalation chemistries.[161] The small market share, compared to other technologies, is also limited due to the small number of manufacturers (Varta, Rayovac, Sony, *etc.*)[162] offering the same type of standard product. For other portable applications, low power uses, and remote-but-yet-portable installations, commercial primary ZAB stacks, with higher nominal capacity, are available from very few manufacturers. For example, Cegasa company (Spain) offers primary ZAB stacks with high nominal capacity (from 100 to 4800 A h packs), used for railway signalling, electric fencing, portable LED lights, mobile warning systems, mobile LED devices, and other remote applications,[163] showing innovative technology applied to many fields outside of the hearing aids. However, the use in larger applications, requiring more power, is limited by the low-rate capability, short lifetime, and leakage of liquid electrolytes of ZABs.

Although focused on electrically rechargeable ZABs, primary batteries are considered here because they can also benefit from the potential progress in GPEs and cathodes, as described in previous sections. For example, natural biopolymer-based GPEs could improve zinc utilization and capacity extraction, replace the separator, and shift from liquid to semi-solid electrolyte to increase durability, apart from being eco-friendly, biodegradable and/or recyclable; the advanced cathode, bifunctional or not, could increase the rate capability, *i.e.*, the maximum current density allowable, reducing the thickness and amount of catalyst required, hence increasing energy and power density.

Nowadays, an interesting and increasing academic field is that of flexible ZABs,[6,164,165] characterized by a multidisciplinary approach where miniaturization, electrochemistry, engineering design, physics, and materials science need to cooperate. Flexible ZABs, primary the most, but also electrically rechargeable, using gelled electrolytes and advanced zinc anodes (powder, paste, and 3D-printed structured foils) could break the market of flexible/wearable electronics or the disposable/wearable non-invasive devices for sensing/detection/biomedical applications.[166–169] Another reason for extending the application of advanced primary ZABs in portable power sources is about future restrictions, environmental concerns, and supply issues of raw materials for LIBs, which could turn the table in favour of aqueous chemistries with no critical raw materials in a post-lithium battery era. Virtually, apart from current catalysts for the OER and carbon-derived materials (coking coal and natural graphite are listed as CRMs), primary ZABs are already CRM-free.

5.2 Secondary ZABs in stationary applications

Available secondary ZABs are nowadays based on mechanical recharge or flowing anode/electrolyte concepts (TRL 6).[161] They present high recharging, recycling, operational and maintenance costs, compared to other technologies for stationary applications, nevertheless they increase the environmental impact of a technology that is virtually eco-friendly by principle. Early developments of high TRL secondary ZABs were historically dedicated to electric vehicles and small stationary applications.[161] Unfortunately, the history of companies in this field (*e.g.*, ReVolt, NantEnergy, and Zinium) includes uncertain success, unclear performances in the field, enthusiastic hyped claims, true liquidations and running outs of the business. A notable, still-running experience is Zinc8[170] among all, proposing a flowing-anode regenerative solution capable of storing energy from 8 to 24 h. The main bottleneck of such configurations is that flowing needs energy, and solid slurries tend to dry and harden quickly, limiting the storage duration, and hence cycling.

Nowadays, electrically rechargeable ZABs are believed to be at TRL 3–4, with a lower rate capability than primary ZABs, and the need for additional components for air management (filters). The niche of small and flexible secondary ZABs for portable devices appears to be more advanced than stationary applications. There is voluminous literature on the topic;[164–167,169] however, higher TRL values seem hard to be achieved in real applications, and reliable commercial products, at any scale, size, or price, are missing, to the best of authors' knowledge.

Electrically rechargeable ZABs would be profitable and desirable in portable as well as stationary, small as well as large (in terms of capacity) applications. Recently, the focus has been on stationary applications because of the low volumetric energy density of zinc.[161] Prospective uses of this technology include renewable energy storage (*i.e.*, solar and wind) in large storage elements for grid support and peak-demand attenuation, small storage elements for residential/single house applications, or hybrid systems together with LIBs to increase the rate capability and response time.[161] Considering recent and future electrocatalyst development for the OER, the advantages of these concepts are clear: they would facilitate the storage of intermittent renewable sources for a short (hours to a few days) to the mid (weeks) term in a cheap, maintenance free, non-CRM-based (or at least with a very small incidence of CRMs) device. To accomplish the goal, electrically rechargeable ZABs would need long cycles (from 6 to 24 h for a discharge/charge cycle), and hence high areal capacities, and higher cycle numbers to approach high total DoD (see Section 4). For stationary applications, more fundamental and solid research, with reliable results, to consolidate a TRL 4, is required to prospectively develop this electrochemical storage direction.

6. Conclusions and final remarks

Electrically rechargeable ZABs are at the border between lab-scale infancy and technological maturity; they need concrete device-level assessment to jump to higher TRLs, getting reliable confidence and a solid basis for sustainable mass production, field application, and market penetration. This would be possible only if extended cyclability and rate capability are

 This journal is © The Royal Society of Chemistry 2022

Open Access Article. Published on 13 2022. Downloaded on 11.07.2024 19:25:14.
This article is licensed under a Creative Commons Attribution-NonCommercial 3.0 Unported Licence.

unlocked. Overall development of materials, components, and cell design is needed because all of them equally participate in setting the device performance. In this perspective, GPEs, bifunctional catalysts/cathodes, and device testing protocols have been discussed. Developing bio-based GPEs, using naturally occurring biopolymers, is ongoing and highly attractive to push the eco-friendliness and sustainable character of ZABs. There is a wide choice of biopolymers and versatile approaches to enhance the physical, chemical, and mechanical properties of hydrogels. Moreover, catalysts with no/less CRMs to design bifunctional cathodes must be further developed and accurately characterized, as well as lab-scale full cells by adopting the correct protocols. The most important aspect is to report suitable metrics and quantitative analysis to assess performances and concrete breakthroughs. Characterization techniques and tools for these purposes are already available and should be systematically applied in future studies. This is fundamental to win the market of portable as well as stationary electrochemical energy storage devices to prevent future crisis due to key materials scarcity, supply chain problems, or environmental issues. The dominance of LIBs hides an unsaid risk of not having a valid alternative technology for energy storage to respond to global concerns about decarbonization, energy cost, and the large use of renewables. ZABs have the theoretical potential to be an alternative to LIBs, reducing the environmental impact, costs, and dependence on non-abundant non-globally distributed sources. A bright future is predicted for this technology if the current gaps and bottlenecks can be solved.

Author contributions

Conceptualization: N. O. V., D. F.; data curation: D. F.; formal analysis: D. F., E. G. G., N. O. V.; investigation: D. F., A. B. M., E. G. G.; funding acquisition: N. O. V.; methodology: N. O. V., D. F.; visualization: D. F., N. O. V.; supervision: N. O. V., M. A.; writing – original draft preparation: all authors; writing – review and editing: all authors.

Conflicts of interest

There are no conflicts to declare.

Acknowledgements

The authors acknowledge the R&D&I project PID2020-117626RA-I00 funded by MCIN/AEI/10.13039/501100011033. E. García Gaitán and N. Ortiz-Vitoriano thank the Basque Government for the Beca Bikaintek 01-AF-W2-2019-00003 and Ramon y Cajal grant (RYC-2020-030104-I) funded by MCIN/AEI/10.13039/501100011033 and by FSE invest in your future, respectively.

References

1 Z. Song, J. Ding, B. Liu, Y. Shen, J. Liu, X. Han, Y. Deng, C. Zhong and W. Hu, *Chem. Eng. J.*, 2022, **429**, 132331.
2 J. F. Parker, J. S. Ko, D. R. Rolison and J. W. Long, *Joule*, 2018, **2**, 2519–2527.
3 N. Radenahmad, R. Khezri, A. A. Mohamad, M. T. Nguyen, T. Yonezawa, A. Somwangthanaroj and S. Kheawhom, *J. Alloys Compd.*, 2021, **883**, 160935.
4 J. Spector and M. V. Olano, **https://www.canarymedia.com/articles/batteries/chart-lithium-prices-are-through-the-roof-this-year**.
5 **https://markets.businessinsider.com/commodities/zinc-price**.
6 J. Fu, Z. P. Cano, M. G. Park, A. Yu, M. Fowler and Z. Chen, *Adv. Mater.*, 2017, **29**, 1604685.
7 N. Borchers, S. Clark, B. Horstmann, K. Jayasayee, M. Juel and P. Stevens, *J. Power Sources*, 2021, **484**, 229309.
8 H. Osgood, S. v Devaguptapu, H. Xu, J. Cho and G. Wu, *Nano Today*, 2016, **11**, 601–625.
9 V. Neburchilov, H. Wang, J. J. Martin and W. Qu, *J. Power Sources*, 2010, **195**, 1271–1291.
10 D. Yang, D. Chen, Y. Jiang, E. H. Ang, Y. Feng, X. Rui and Y. Yu, *Carbon Energy*, 2021, **3**, 50–65.
11 X. G. Zhang, *J. Power Sources*, 2006, **163**, 591–597.
12 J. F. Parker, C. N. Chervin, E. S. Nelson, D. R. Rolison and J. W. Long, *Energy Environ. Sci.*, 2014, **7**, 1117–1124.
13 D. Stock, S. Dongmo, J. Janek and D. Schröder, *ACS Energy Lett.*, 2019, **4**, 1287–1300.
14 J. Zheng and L. A. Archer, *Sci. Adv.*, 2021, **7**(2), eabe0219.
15 S. Lorca, F. Santos and A. J. Fernández Romero, *Polymers*, 2020, **12**, 2812.
16 E. Lizundia and D. Kundu, *Adv. Funct. Mater.*, 2021, **31**, 2005646.
17 F. Mahlendorf, A. Heinzel, C. Mueller and D. Fuchs, *Electrochemical Power Sources: Fundamentals, Systems, and Applications*, Elsevier, 2021, pp. 99–123.
18 L. Jörissen, *Electrochemical Power Sources: Fundamentals, Systems, and Applications*, Elsevier, 2021, pp. 81–97.
19 M. Krebs, H.-U. Reichardt, R. Sojka and P. Stevens, *Electrochemical Power Sources: Fundamentals, Systems, and Applications*, Elsevier, 2021, pp. 217–245.
20 Y. He, W. Shang, M. Ni, Y. Huang, H. Zhao and P. Tan, *Chem. Eng. J.*, 2022, **427**, 130862.
21 S. Velraj, A. K. Estes, B. L. Bates and J. H. Zhu, *Electrochim. Acta*, 2018, **292**, 446–457.
22 S. Möller, S. Barwe, S. Dieckhöfer, J. Masa, C. Andronescu and W. Schuhmann, *ChemElectroChem*, 2020, **7**, 2680–2686.
23 Y. J. Min, S. J. Oh, M. S. Kim, J. H. Choi and S. Eom, *J. Appl. Electrochem.*, 2018, **48**, 405–413.
24 S. S. Shinde, C. H. Lee, J.-Y. Jung, N. K. Wagh, S.-H. Kim, D.-H. Kim, C. Lin, S. U. Lee and J.-H. Lee, *Energy Environ. Sci.*, 2019, **12**, 727–738.
25 A. B. Balaji, H. Pakalapati, M. Khalid, R. Walvekar and H. Siddiqui, *Biodegradable and Biocompatible Polymer Composites*, Elsevier, 2018, pp. 3–32.
26 R. Rebelo, M. Fernandes and R. Fangueiro, *Procedia Eng.*, 2017, **200**, 236–243.
27 Q. Wu, Y. Wang and G.-Q. Chen, *Artif. Cells, Blood Substitutes, Biotechnol.*, 2009, **37**, 1–12.

Open Access Article. Published on 13 2022. Downloaded on 11.07.2024 19:25:14.
This article is licensed under a Creative Commons Attribution-NonCommercial 3.0 Unported Licence.

28 J. Pandey, Biopolymers and Their Application in Wastewater Treatment, in *Emerging Eco-friendly Green Technologies for Wastewater Treatment*, ed. R. Bharagava, 2020, pp. 245–266.
29 G. Robertson, *Environmentally Compatible Food Packaging*, Elsevier, 2008, pp. 3–28.
30 J. N. de Freitas, J. E. Benedetti, F. S. Freitas, A. F. Nogueira and M. A. de Paoli, *Polymer Electrolytes*, Elsevier, 2010, pp. 381–430.
31 H. Tian, Z. Tang, X. Zhuang, X. Chen and X. Jing, *Prog. Polym. Sci.*, 2012, **37**, 237–280.
32 K. H. Hong, *Polym. Bull.*, 2017, **74**, 2861–2872.
33 C. Wang, T. Yokota and T. Someya, *Chem. Rev.*, 2021, **121**, 2109–2146.
34 K. Varaprasad, G. M. Raghavendra, T. Jayaramudu, M. M. Yallapu and R. Sadiku, *Mater. Sci. Eng., C*, 2017, **79**, 958–971.
35 T. N. T. Tran, D. Aasen, D. Zhalmuratova, M. Labbe, H. Chung and D. G. Ivey, *Batteries Supercaps*, 2020, **3**, 917–927.
36 B. Guo and P. X. Ma, *Sci. China: Chem.*, 2014, **57**, 490–500.
37 J. Kundu, F. Pati, Y. Hun Jeong and D.-W. Cho, *Biofabrication*, Elsevier, 2013, pp. 23–46.
38 X. Fu and W. Zhong, *Adv. Energy Mater.*, 2019, **9**, 1901774.
39 C.-C. Yang, J. M. Yang and C.-Y. Wu, *J. Power Sources*, 2009, **191**, 669–677.
40 O. Kwon, H. J. Hwang, Y. Ji, O. S. Jeon, J. P. Kim, C. Lee and Y. G. Shul, *Sci. Rep.*, 2019, **9**, 3175.
41 Y. Zhang, C. Li, X. Cai, J. Yao, M. Li, X. Zhang and Q. Liu, *Electrochim. Acta*, 2016, **220**, 635–642.
42 O. E. Philippova and A. R. Khokhlov, *Polymer Science: A Comprehensive Reference*, Elsevier, 2012, pp. 339–366.
43 Y. Wei, M. Wang, N. Xu, L. Peng, J. Mao, Q. Gong and J. Qiao, *ACS Appl. Mater. Interfaces*, 2018, **10**, 29593–29598.
44 J. Zhang, J. Fu, X. Song, G. Jiang, H. Zarrin, P. Xu, K. Li, A. Yu and Z. Chen, *Adv. Energy Mater.*, 2016, **6**, 1600476.
45 F. Ullah, M. B. H. Othman, F. Javed, Z. Ahmad and H. Md Akil, *Mater. Sci. Eng., C*, 2015, **57**, 414–433.
46 G. M. Wu, S. J. Lin and C. C. Yang, *J. Membr. Sci.*, 2006, **280**, 802–808.
47 M. Wang, N. Xu, J. Fu, Y. Liu and J. Qiao, *J. Mater. Chem. A*, 2019, **7**, 11257–11264.
48 J. Fu, D. U. Lee, F. M. Hassan, L. Yang, Z. Bai, M. G. Park and Z. Chen, *Adv. Mater.*, 2015, **27**, 5617–5622.
49 N. Zhao, F. Wu, Y. Xing, W. Qu, N. Chen, Y. Shang, M. Yan, Y. Li, L. Li and R. Chen, *ACS Appl. Mater. Interfaces*, 2019, **11**, 15537–15542.
50 I. Chiulan, E. B. Heggset, Ş. I. Voicu and G. Chinga-Carrasco, *Biomacromolecules*, 2021, **22**, 1795–1814.
51 S. Bastani and M. Mohseni, *Handbook of Nanoceramic and Nanocomposite Coatings and Materials*, Elsevier, 2015, pp. 155–182.
52 M. T. Tsehaye, F. Alloin, C. Iojoiu, R. A. Tufa, D. Aili, P. Fischer and S. Velizarov, *J. Power Sources*, 2020, **475**, 228689.
53 E. L. Dewi, K. Oyaizu, H. Nishide and E. Tsuchida, *J. Power Sources*, 2003, **115**, 149–152.
54 J. Fu, J. Zhang, X. Song, H. Zarrin, X. Tian, J. Qiao, L. Rasen, K. Li and Z. Chen, *Energy Environ. Sci.*, 2016, **9**, 663–670.
55 *Biopolymer Membranes and Films*, ed. M. Agostini de Moraes, C. Ferreira da Silva and R. Silveira Vieira, Elsevier, 1st edn, 2020.
56 X. Zhu, K. Wang, Y. Xu, G. Zhang, S. Li, C. Li, X. Zhang, X. Sun, X. Ge and Y. Ma, *Energy Storage Mater.*, 2021, **36**, 291–308.
57 E. Raphael, C. O. Avellaneda, M. A. Aegerter, M. M. Silva and A. Pawlicka, *Mol. Cryst. Liq. Cryst.*, 2012, **554**, 264–272.
58 K. Lu, T. Jiang, H. Hu and M. Wu, *Front. Chem.*, 2020, **8**, 546728.
59 M. J. Tan, B. Li, P. Chee, X. Ge, Z. Liu, Y. Zong and X. J. Loh, *J. Power Sources*, 2018, **400**, 566–571.
60 A. Poosapati, E. Jang, D. Madan, N. Jang, L. Hu and Y. Lan, *MRS Commun.*, 2019, **9**, 122–128.
61 Q. Wang, H. Miao, S. Sun, Y. Xue and Z. Liu, *Chem. – Eur. J.*, 2018, **24**, 14816–14823.
62 Y. Zuo, K. Wang, M. Wei, S. Zhao, P. Zhang and P. Pei, *Cell Rep. Phys. Sci.*, 2022, **3**, 100687.
63 J. Zhang, T. Zhou, J. Qiao, Y. Liu and J. Zhang, *Electrochim. Acta*, 2013, **111**, 351–358.
64 J. Qiao, J. Zhang and J. Zhang, *J. Power Sources*, 2013, **237**, 1–4.
65 C.-C. Yang, S.-J. Lin and S.-T. Hsu, *J. Power Sources*, 2003, **122**, 210–218.
66 M. N. Masri, M. F. M. Nazeri and A. A. Mohamad, Sago Gel Polymer Electrolyte for Zinc-Air Battery, *5th FORUM ON NEW MATERIALS PART A*, 2010, vol. 72, pp. 305–308, DOI: **10.4028/www.scientific.net/AST.72.305**.
67 J. Lu, P. Jaumaux, T. Wang, C. Wang and G. Wang, *J. Mater. Chem. A*, 2021, **9**, 24175–24194.
68 J. Hur, K. Im, S. W. Kim, J. Kim, D.-Y. Chung, T.-H. Kim, K. H. Jo, J. H. Hahn, Z. Bao, S. Hwang and N. Park, *ACS Nano*, 2014, **8**, 10066–10076.
69 S. Y. Liew, J. C. Juan, C. W. Lai, G.-T. Pan, T. C.-K. Yang and T. K. Lee, *Ionics*, 2019, **25**, 1291–1301.
70 U. Bhardwaj, A. Sharma, A. Mathur, A. Halder and H. S. Kushwaha, *Electrochem. Sci. Adv.*, 2022, **2**(3), e202100056.
71 J. Park, M. Park, G. Nam, J. Lee and J. Cho, *Adv. Mater.*, 2015, **27**, 1396–1401.
72 Z. Song, J. Ding, B. Liu, X. Liu, X. Han, Y. Deng, W. Hu and C. Zhong, *Adv. Mater.*, 2020, **32**, 1908127.
73 J. Enrione, C. Char, M. Pepczynska, C. Padilla, A. González-Muñoz, Y. Olguín, C. Quinzio, L. Iturriaga and P. Díaz-Calderón, *Polymers*, 2020, **12**, 1587.
74 F. A. Johnston-Banks, *Food Gels*, Springer Netherlands, Dordrecht, 1990, pp. 233–289.
75 R. A. S. N. Ranasinghe, W. L. I. Wijesekara, P. R. D. Perera, S. A. Senanayake, M. M. Pathmalal and R. A. U. J. Marapana, *Food Rev. Int.*, 2022, **38**, 812–855.
76 F. Colò, F. Bella, J. R. Nair, M. Destro and C. Gerbaldi, *Electrochim. Acta*, 2015, **174**, 185–190.
77 Y. Zhang, Y. Chen, X. Li, M. Alfred, D. Li, F. Huang and Q. Wei, *J. Power Sources*, 2021, **482**, 228963.

 This journal is © The Royal Society of Chemistry 2022

Open Access Article. Published on 13 2022. Downloaded on 11.07.2024 19:25:14.
This article is licensed under a Creative Commons Attribution-NonCommercial 3.0 Unported Licence.

78 J. Fu, F. M. Hassan, J. Li, D. U. Lee, A. R. Ghannoum, G. Lui, Md. A. Hoque and Z. Chen, *Adv. Mater.*, 2016, **28**, 6421–6428.
79 F. Meng, H. Zhong, D. Bao, J. Yan and X. Zhang, *J. Am. Chem. Soc.*, 2016, **138**, 10226–10231.
80 D. Lee, H.-W. Kim, J.-M. Kim, K.-H. Kim and S.-Y. Lee, *ACS Appl. Mater. Interfaces*, 2018, **10**, 22210–22217.
81 S. Peng, X. Han, L. Li, S. Chou, D. Ji, H. Huang, Y. Du, J. Liu and S. Ramakrishna, *Adv. Energy Mater.*, 2018, **8**, 1800612.
82 T. N. T. Tran, H.-J. Chung and D. G. Ivey, *Electrochim. Acta*, 2019, **327**, 135021.
83 S. S. Shinde, C. H. Lee, J.-Y. Yu, D.-H. Kim, S. U. Lee and J.-H. Lee, *ACS Nano*, 2018, **12**, 596–608.
84 A. R. M. Zahid, M. N. Masri, M. H. Hussin and M. B. A. Bakar, *AIP Conf. Proc.*, 2018, **2030**, 020278.
85 D. Bresser, D. Buchholz, A. Moretti, A. Varzi and S. Passerini, *Energy Environ. Sci.*, 2018, **11**, 3096–3127.
86 S. Hosseini, S. Masoudi Soltani and Y.-Y. Li, *Chem. Eng. J.*, 2021, **408**, 127241.
87 P. Zhang, K. Wang, P. Pei, Y. Zuo, M. Wei, X. Liu, Y. Xiao and J. Xiong, *Mater. Today Chem.*, 2021, **21**, 100538.
88 Y. Zhou, J. Pan, X. Ou, Q. Liu, Y. Hu, W. Li, R. Wu, J. Wen and F. Yan, *Adv. Energy Mater.*, 2021, **11**, 2102047.
89 Z. Pei, L. Ding, C. Wang, Q. Meng, Z. Yuan, Z. Zhou, S. Zhao and Y. Chen, *Energy Environ. Sci.*, 2021, **14**, 4926–4935.
90 Z. Pei, Z. Yuan, C. Wang, S. Zhao, J. Fei, L. Wei, J. Chen, C. Wang, R. Qi, Z. Liu and Y. Chen, *Angew. Chem., Int. Ed.*, 2020, **59**, 4793–4799.
91 X. Liu, X. Fan, B. Liu, J. Ding, Y. Deng, X. Han, C. Zhong and W. Hu, *Adv. Mater.*, 2021, **33**, 2006461.
92 J. Pang, R. G. Mendes, A. Bachmatiuk, L. Zhao, H. Q. Ta, T. Gemming, H. Liu, Z. Liu and M. H. Rummeli, *Chem. Soc. Rev.*, 2019, **48**, 72–133.
93 B. Anasori, M. R. Lukatskaya and Y. Gogotsi, *Nat. Rev. Mater.*, 2017, **2**, 16098.
94 E. Antolini, *Renewable Sustainable Energy Rev.*, 2016, **58**, 34–51.
95 D. Liu, Y. Tong, X. Yan, J. Liang and S. X. Dou, *Batteries Supercaps*, 2019, **2**, 743–765.
96 Y. Dai, J. Yu, C. Cheng, P. Tan and M. Ni, *Chem. Eng. J.*, 2020, **397**, 125516.
97 R. Cao, J.-S. Lee, M. Liu and J. Cho, *Adv. Energy Mater.*, 2012, **2**, 816–829.
98 Z. Chen, J.-Y. Choi, H. Wang, H. Li and Z. Chen, *J. Power Sources*, 2011, **196**, 3673–3677.
99 F. Cheng and J. Chen, *Chem. Soc. Rev.*, 2012, **41**, 2172.
100 Z. Chen, A. Yu, R. Ahmed, H. Wang, H. Li and Z. Chen, *Electrochim. Acta*, 2012, **69**, 295–300.
101 Y. Li, M. Gong, Y. Liang, J. Feng, J.-E. Kim, H. Wang, G. Hong, B. Zhang and H. Dai, *Nat. Commun.*, 2013, **4**, 1805.
102 G. Du, X. Liu, Y. Zong, T. S. A. Hor, A. Yu and Z. Liu, *Nanoscale*, 2013, **5**, 4657.
103 X. Ge, Y. Liu, F. W. T. Goh, T. S. A. Hor, Y. Zong, P. Xiao, Z. Zhang, S. H. Lim, B. Li, X. Wang and Z. Liu, *ACS Appl. Mater. Interfaces*, 2014, **6**, 12684–12691.
104 M. Prabu, P. Ramakrishnan and S. Shanmugam, *Electrochem. Commun.*, 2014, **41**, 59–63.
105 X. Liu, M. Park, M. G. Kim, S. Gupta, G. Wu and J. Cho, *Angew. Chem., Int. Ed.*, 2015, **54**, 9654–9658.
106 G. Li, X. Wang, J. Fu, J. Li, M. G. Park, Y. Zhang, G. Lui and Z. Chen, *Angew. Chem., Int. Ed.*, 2016, **55**, 4977–4982.
107 L.-N. Han, L.-B. Lv, Q.-C. Zhu, X. Wei, X.-H. Li and J.-S. Chen, *J. Mater. Chem. A*, 2016, **4**, 7841–7847.
108 P.-C. Li, Y.-J. Chien and C.-C. Hu, *J. Power Sources*, 2016, **313**, 37–45.
109 X. Han, X. Wu, C. Zhong, Y. Deng, N. Zhao and W. Hu, *Nano Energy*, 2017, **31**, 541–550.
110 Q. Wang, L. Shang, R. Shi, X. Zhang, Y. Zhao, G. I. N. Waterhouse, L.-Z. Wu, C.-H. Tung and T. Zhang, *Adv. Energy Mater.*, 2017, **7**, 1700467.
111 Q. Wang, Y. Lei, Z. Chen, N. Wu, Y. Wang, B. Wang and Y. Wang, *J. Mater. Chem. A*, 2018, **6**, 516–526.
112 S. S. Shinde, C. H. Lee, J.-Y. Jung, N. K. Wagh, S.-H. Kim, D.-H. Kim, C. Lin, S. U. Lee and J.-H. Lee, *Energy Environ. Sci.*, 2019, **12**, 727–738.
113 K. Wu, L. Zhang, Y. Yuan, L. Zhong, Z. Chen, X. Chi, H. Lu, Z. Chen, R. Zou, T. Li, C. Jiang, Y. Chen, X. Peng and J. Lu, *Adv. Mater.*, 2020, **32**, 2002292.
114 V. Jose, H. Hu, E. Edison, W. Manalastas, H. Ren, P. Kidkhunthod, S. Sreejith, A. Jayakumar, J. M. V. Nsanzimana, M. Srinivasan, J. Choi and J. Lee, *Small Methods*, 2021, **5**, 2000751.
115 B. J. Kim, D. U. Lee, J. Wu, D. Higgins, A. Yu and Z. Chen, *J. Phys. Chem. C*, 2013, **117**, 26501–26508.
116 H.-W. Liang, X. Zhuang, S. Brüller, X. Feng and K. Müllen, *Nat. Commun.*, 2014, **5**, 4973.
117 J. Zhang, Z. Zhao, Z. Xia and L. Dai, *Nat. Nanotechnol.*, 2015, **10**, 444–452.
118 Y. Jia, L. Zhang, A. Du, G. Gao, J. Chen, X. Yan, C. L. Brown and X. Yao, *Adv. Mater.*, 2016, **28**, 9532–9538.
119 H. bin Yang, J. Miao, S.-F. Hung, J. Chen, H. B. Tao, X. Wang, L. Zhang, R. Chen, J. Gao, H. M. Chen, L. Dai and B. Liu, *Sci. Adv.*, 2016, **2**(4), e1501122.
120 C. Tang, B. Wang, H. Wang and Q. Zhang, *Adv. Mater.*, 2017, **29**, 1703185.
121 P. Chen, T. Zhou, L. Xing, K. Xu, Y. Tong, H. Xie, L. Zhang, W. Yan, W. Chu, C. Wu and Y. Xie, *Angew. Chem., Int. Ed.*, 2017, **56**, 610–614.
122 C. Su, H. Cheng, W. Li, Z. Liu, N. Li, Z. Hou, F. Bai, H. Zhang and T. Ma, *Adv. Energy Mater.*, 2017, **7**, 1602420.
123 S. S. Shinde, C.-H. Lee, A. Sami, D.-H. Kim, S.-U. Lee and J.-H. Lee, *ACS Nano*, 2017, **11**, 347–357.
124 X. Peng, L. Zhang, Z. Chen, L. Zhong, D. Zhao, X. Chi, X. Zhao, L. Li, X. Lu, K. Leng, C. Liu, W. Liu, W. Tang and K. P. Loh, *Adv. Mater.*, 2019, **31**, 1900341.
125 Y. Zheng, H. Song, S. Chen, X. Yu, J. Zhu, J. Xu, K. A. I. Zhang, C. Zhang and T. Liu, *Small*, 2020, **16**, 2004342.
126 Y. Wang, N. Xu, R. He, L. Peng, D. Cai and J. Qiao, *Appl. Catal., B*, 2021, **285**, 119811.
127 X. Li, W. Qu, J. Zhang and H. Wang, *J. Electrochem. Soc.*, 2011, **158**, A597.

Open Access Article. Published on 13 2022. Downloaded on 11.07.2024 19:25:14.
This article is licensed under a Creative Commons Attribution-NonCommercial 3.0 Unported Licence.

128 Z. Chen, A. Yu, D. Higgins, H. Li, H. Wang and Z. Chen, *Nano Lett.*, 2012, **12**, 1946–1952.
129 K.-N. Jung, J.-H. Jung, W. bin Im, S. Yoon, K.-H. Shin and J.-W. Lee, *ACS Appl. Mater. Interfaces*, 2013, **5**, 9902–9907.
130 D. U. Lee, H. W. Park, M. G. Park, V. Ismayilov and Z. Chen, *ACS Appl. Mater. Interfaces*, 2015, **7**, 902–910.
131 K. Lopez, G. Park, H.-J. Sun, J.-C. An, S. Eom and J. Shim, *J. Appl. Electrochem.*, 2015, **45**, 313–323.
132 M. Prabu, P. Ramakrishnan, P. Ganesan, A. Manthiram and S. Shanmugam, *Nano Energy*, 2015, **15**, 92–103.
133 A. Vignesh, M. Prabu and S. Shanmugam, *ACS Appl. Mater. Interfaces*, 2016, **8**, 6019–6031.
134 Y. Bu, O. Gwon, G. Nam, H. Jang, S. Kim, Q. Zhong, J. Cho and G. Kim, *ACS Nano*, 2017, **11**, 11594–11601.
135 H. Miao, Z. Wang, Q. Wang, S. Sun, Y. Xue, F. Wang, J. Zhao, Z. Liu and J. Yuan, *Energy*, 2018, **154**, 561–570.
136 H. Lee, O. Gwon, C. Lim, J. Kim, O. Galindev and G. Kim, *ChemElectroChem*, 2019, **6**, 3154–3159.
137 C. Zhao, X. Zhang, M. Yu, A. Wang, L. Wang, L. Xue, J. Liu, Z. Yang and W. Wang, *Adv. Mater.*, 2020, **32**, 2006145.
138 X. Shi, Y. Deng, L. Zhao, Y. Gong, R. Wang, H. Wang and B. He, *Electrochim. Acta*, 2021, **391**, 138951.
139 European Commission, Critical raw materials resilience: charting a path towards greater security and sustainability, **https://ec.europa.eu/docsroom/documents/42849/attachments/2/translations/en/renditions/native**, (accessed 18 February 2022).
140 A. J. Bard and L. R. Faulkner, *Electrochemical Methods: Fundamentals and Applications*, John Wiley & Sons, Inc, New York, 2 edn, 2001.
141 C. Wei, R. R. Rao, J. Peng, B. Huang, I. E. L. Stephens, M. Risch, Z. J. Xu and Y. Shao-Horn, *Adv. Mater.*, 2019, **31**, 1806296.
142 N. Elgrishi, K. J. Rountree, B. D. McCarthy, E. S. Rountree, T. T. Eisenhart and J. L. Dempsey, *J. Chem. Educ.*, 2018, **95**, 197–206.
143 C. A. Campos-Roldán, R. G. González-Huerta and N. Alonso-Vante, *J. Electrochem. Soc.*, 2018, **165**, J3001–J3007.
144 Y. Wu and Y. Nabae, *Curr. Opin. Electrochem.*, 2021, **25**, 100633.
145 J. Suntivich, H. A. Gasteiger, N. Yabuuchi, H. Nakanishi, J. B. Goodenough and Y. Shao-Horn, *Nat. Chem.*, 2011, **3**, 546–550.
146 J. Suntivich, K. J. May, H. A. Gasteiger, J. B. Goodenough and Y. Shao-Horn, *Science*, 1979, **2011**(334), 1383–1385.
147 C. Wei, Z. Feng, G. G. Scherer, J. Barber, Y. Shao-Horn and Z. J. Xu, *Adv. Mater.*, 2017, **29**, 1606800.
148 I. Yamada, A. Takamatsu, K. Asai, T. Shirakawa, H. Ohzuku, A. Seno, T. Uchimura, H. Fujii, S. Kawaguchi, K. Wada, H. Ikeno and S. Yagi, *J. Phys. Chem. C*, 2018, **122**, 27885–27892.
149 J. A. Dias, M. A. S. Andrade, H. L. S. Santos, M. R. Morelli and L. H. Mascaro, *ChemElectroChem*, 2020, **7**, 3173–3192.
150 I. Yamada, A. Takamatsu, K. Asai, T. Shirakawa, H. Ohzuku, A. Seno, T. Uchimura, H. Fujii, S. Kawaguchi, K. Wada, H. Ikeno and S. Yagi, *J. Phys. Chem. C*, 2018, **122**, 27885–27892.
151 J. J. Martin, V. Neburchilov, H. Wang and W. Qu, 2009 IEEE Electrical Power & Energy Conference (EPEC), IEEE, 2009, pp. 1–6.
152 Y. Zhong, X. Xu, P. Liu, R. Ran, S. P. Jiang, H. Wu and Z. Shao, *Adv. Energy Mater.*, 2020, **10**, 2002992.
153 Y. Dai, J. Yu, P. Tan, C. Cheng, T. Liu, S. Zhao, Z. Shao, T. Zhao and M. Ni, *J. Power Sources*, 2022, **525**, 231108.
154 J. Yu, B. Li, C. Zhao, J. Liu and Q. Zhang, *Adv. Mater.*, 2020, **32**, 1908488.
155 S. Askari, D. Mariotti, R. McGlynn and J. Benedikt, *Energy Technol.*, 2021, **9**, 2000999.
156 X. X. Wang, X. Yang, H. Liu, T. Han, J. Hu, H. Li and G. Wu, *Small Struct.*, 2022, **3**, 2100103.
157 X. Hu, X. Tian, Y.-W. Lin and Z. Wang, *RSC Adv.*, 2019, **9**, 31563–31571.
158 S. Dongmo, J. J. A. Kreissl, K. Miyazaki, T. Abe, T.-H. You, C.-C. Hu and D. Schröder, *Sci. Data*, 2020, **7**, 395.
159 J. F. Parker, C. N. Chervin, E. S. Nelson, D. R. Rolison and J. W. Long, *Energy Environ. Sci.*, 2014, **7**, 1117–1124.
160 Y. Huang, Z. Li, Z. Pei, Z. Liu, H. Li, M. Zhu, J. Fan, Q. Dai, M. Zhang, L. Dai and C. Zhi, *Adv. Energy Mater.*, 2018, **8**, 1802288.
161 M. Krebs, H.-U. Reichardt, R. Sojka and P. Stevens, *Electrochemical Power Sources: Fundamentals, Systems, and Applications*, Elsevier, 2021, pp. 217–245.
162 Zinc air battery technical specifications (by brand), **https://www.microbattery.com/zinc-air-battery-specs**, (accessed 4 May 2022).
163 Cegasa Zinc air alkaline, **https://www.cegasa.com/en/ez8**, (accessed 4 May 2022).
164 P. Tan, B. Chen, H. Xu, H. Zhang, W. Cai, M. Ni, M. Liu and Z. Shao, *Energy Environ. Sci.*, 2017, **10**, 2056–2080.
165 Y. Xu, X. Xu, M. Guo, G. Zhang and Y. Wang, *Front. Chem.*, 2022, **10**, 827563.
166 J. Zhou, J. Cheng, B. Wang, H. Peng and J. Lu, *Energy Environ. Sci.*, 2020, **13**, 1933–1970.
167 S. Lorca, F. Santos and A. J. Fernández Romero, *Polymers*, 2020, **12**, 2812.
168 P. Bocchetta, D. Frattini, S. Ghosh, A. M. V. Mohan, Y. Kumar and Y. Kwon, *Materials*, 2020, **13**, 2733.
169 P. Zhang, K. Wang, P. Pei, Y. Zuo, M. Wei, X. Liu, Y. Xiao and J. Xiong, *Mater. Today Chem.*, 2021, **21**, 100538.
170 Zinc8 storage solutions, **https://www.zinc8energy.com/**, (accessed 5 May 2022).

 This journal is © The Royal Society of Chemistry 2022